

We are IntechOpen, the world's leading publisher of Open Access books Built by scientists, for scientists

6,900

Open access books available

186,000

International authors and editors

200M

Downloads

Our authors are among the

154

Countries delivered to

TOP 1%

most cited scientists

12.2%

Contributors from top 500 universities



WEB OF SCIENCE™

Selection of our books indexed in the Book Citation Index
in Web of Science™ Core Collection (BKCI)

Interested in publishing with us?
Contact book.department@intechopen.com

Numbers displayed above are based on latest data collected.
For more information visit www.intechopen.com



Estimation and Uncertainty Assessment of Surface Microclimate Indicators at Local Scale Using Airborne Infrared Thermography and Multispectral Imagery

Serge Olivier Kotchi, Nathalie Barrette,
Alain A. Viau, Jae-Dong Jang, Valéry Gond and
Mir Abolfazl Mostafavi

Additional information is available at the end of the chapter

<http://dx.doi.org/10.5772/64527>

Abstract

A precise estimation and the characterization of the spatial variability of microclimate conditions (MCCs) are essential for risk assessment and site-specific management of vector-borne diseases and crop pests. The objective of this study was to estimate at local scale, and assess the uncertainties of Surface Microclimate Indicators (SMIs) derived from airborne infrared thermography and multispectral imaging. SMIs including Surface Temperature (ST) were estimated in southern Quebec, Canada. The formulation of their uncertainties was based on in-situ observations and the law of propagation of uncertainty. SMIs showed strong local variability and intra-plot variability of MCCs in the study area. The ST values ranged from 290 K to 331 K. They varied more than 17 K on vegetable crop fields. The correlation between ST and in-situ observations was very high ($r = 0.99$, $p = 0.010$). The uncertainty and the bias of ST compared to in-situ observations were 0.73 K and ± 1.42 K respectively. This study demonstrated that very high spatial resolution multispectral imaging and infrared thermography present a good potential for the characterization of the MCCs that govern the abundance and the behavior of disease vectors and crop pests in a given area.

Keywords: airborne remote sensing, infrared thermography, microclimate indicators, uncertainty, local scale, crop, pests and diseases

1. Introduction

Microclimates which are defined by agrometeorological conditions are key factors governing crop development and growth. They influence the abundance, development, and behavior of diseases and pests which can significantly reduce crop yield [1–6]. A regular use of pesticides for pest control can result, along with the risk to environmental and human health that pesticides pose. Microclimate variability induced by agrometeorological conditions represents around 80% of the variability of agricultural production [7]. These conditions are defined through variables such as the amount of vegetation, surface temperature, surface moisture, air temperature (AT), relative humidity (RH), solar radiation, evapotranspiration, wind speed and direction, rainfall, etc. Indicators such as percent vegetation cover (PVC) and leaf area index (LAI) [8, 9], duration of leaf wetness [2, 10], thermal units [11], degree days, vapor pressure deficit [7, 11, 12], potential evapotranspiration [13], water stress indices [12, 14, 15], drought indices [16], precipitation indices [17], etc., are related to these variables, and they are used to quantify and monitor agrometeorological and microclimate conditions on a given territory. They are also used to identify appropriate times in the management of various agricultural practices like sowing, irrigation, disease and pest screening, applying manure and pesticides, and harvesting. These variables and their related indicators are defined in this work as microclimate indicators (MCIs). MCIs, which are related to vegetation, temperature, and humidity levels, are considered critical indicators [18–24] and are used for the prediction and management of agricultural practices. They are the main input variables of models used to estimate other MCIs [2, 7, 25], models of growth and yield forecasting [25–28], models of disease and pest predictions [10, 23, 29], and models of climate prediction and adaptation to climate change [30, 31].

Several MCIs are commonly observed using weather stations [18, 32, 33] or in situ sensors [28, 34]. However, data from weather stations are point data that represent the specific conditions of the observing site. Their spatial representation on a larger area is not always valid [2, 7] because of the spatial heterogeneity of landscape and microclimate conditions [35]. The low number of weather stations and their generally sparse geographical distribution does not often allow for the characterization of the spatial variability of a microclimate within a given area [18, 32, 33, 36]. The cost and the maintenance of a more densified weather station networks to ensure better characterization of the spatial variability of microclimates is very high and could not be supported by the users [32]. In addition, meteorological data are often missing or erroneous in many parts of the world [7, 34, 36], which limits the application of simulation models [37, 38] and the management of agricultural practices. Some MCIs are considered secondary variables and are not commonly observed by weather stations [7], and punctual observations are not appropriate because of their large spatial variability [29, 39, 40]. Compared to MCIs related to atmospheric conditions (air temperature, relative humidity), those related to surface conditions (surface microclimate indicators, SMIs) like vegetation amount, surface temperature (ST), surface moisture and leaf wetness duration are often not observed by weather stations [10, 25, 41]. These SMIs are more directly related to microclimate conditions which affect water status and crop growth as well as the abundance, behavior and development of crop pests and diseases. And, weather stations where these SMIs are actually observed

frequently report missing or erroneous data due to equipment failure [25]. Punctual in situ observations over crop fields to address the lack of data on those SMIs are time and resource consuming, and they do not always result in a good characterization of their spatial variability [42]. Finally, for some of these SMIs, like leaf wetness, there is no commonly accepted standard for their measurement [2]. Due to all these limitations, weather station networks are not always able to meet the requirements for characterization of microclimate conditions in agriculture, or more specifically in precision agriculture and site-specific pest management [40]. This also concerns several other applications which require the characterization of the microclimate conditions.

While SMIs related to surface conditions are less frequently observed by weather stations, they are the primary variables derived from satellite images. Thus, the estimation of SMIs using satellite images overcomes the problem of sparse meteorological station networks and the nonavailability of meteorological data [18]. Some agricultural management programs are based on MCIs estimated by satellite images, where meteorological ground station data are not available [39]. These images offer a unique advantage for the estimation and the monitoring of microclimate conditions in the soil-vegetation-atmosphere interface over vast territories and at different spatial and temporal resolutions [43–46]. The spatial density of data derived from satellite images exceeds that of observations from weather stations. These data allow a better characterization of the spatial variability of microclimate conditions. Compared to point data acquired in fields, they are less costly in time and money [34]. Vegetation indices (VIs) derived from satellite images are used to estimate indicators of the amount of vegetation like percent vegetation cover (PVC) [8, 9, 47, 48] and leaf area index (LAI) [28, 49–51]. The normalized difference vegetation index (NDVI) is the best known and most widely used VI [11, 28, 34, 45, 46, 51, 52]. It is used in many other applications including estimating biophysical variables such as photosynthetically active radiation (PAR) and evapotranspiration [53, 54], monitoring crop growth and development [39, 46, 52], yield forecasting [55–57], and drought monitoring [16, 34, 58]. Surface temperature (ST) is a key variable to understanding and to characterizing heat and water exchanges between the surface and the atmosphere [20, 59, 60]. It can be estimated using several Earth observation systems like GOES, MSG/SEVIRI, NOAA/AVHRR, Terra, Aqua/MODIS, ASTER, and Landsat-8/TIRS. ST is used for the estimation of other MCIs such as air temperature [18] and evapotranspiration [37], for the detection of water deficits and the monitoring of drought conditions [16, 61], and for risk assessment of the occurrence of diseases and pests [32]. For example, the temperature condition index (TCI), based on the ST derived from satellite images, is one of the most used to track drought conditions and their impact on regional and global scales [16]. Variations of surface moisture in the short and long term and its impact on vegetation can be monitored using stress indices based on ST and IVs derived from satellite images [56]. The TVDI is one of the most used indices to estimate surface moisture [21, 24, 62, 63]. Chen et al. [64] used the TVDI estimated using MODIS images to characterize the spatial variability of surface moisture and to link it with rice farming systems in the Mekong Delta, Vietnam. Holzman et al. [56] also used the TVDI derived from MODIS images to estimate soil water availability and to assess crop yield at the regional scale.

SMIs which are derived from satellite images have a good potential to be used in regional agro-meteorological systems [35]. Several products related to surface temperature and to vegetation indices, such as those of MODIS, are also available in the form of time series. These products are frequently used to study climate and other dynamic phenomena in space and time [65]. However, applications of SMIs are limited either by the low spatial resolution or by the low temporal resolution of Earth observation systems which are used [60]. ST is derived from systems such as GOES and MSG/SEVIRI with a very high temporal resolution (15 min). However, these systems are characterized by a very low spatial resolution (3–5 km). Sensors like MODIS and AVHRR, which are mostly used to estimate surface temperature in many applications, are characterized by a high temporal resolution (1 day), but are associated with a low spatial resolution (1 km). Earth observation systems including Landsat-5/TM, Landsat-7/ETM+, and Landsat-8/TIRS are those with the best spatial resolution in thermal bands (120, 60, and 100 m, respectively). However, they are limited by a very low temporal resolution (16 days). The low spatial resolution satellite images used to estimate SMIs often lead to mixed pixels that combine different elements like bare soil, vegetation, water, impervious surfaces, and clouds, especially in environments with a strong spatial heterogeneity [32, 48, 59, 66]. These mixed pixels could lead to significant errors in the estimation of SMIs [32, 66]. This low spatial resolution also makes it difficult to link data from satellite images and data collected in the field [45, 48]. Moreover, the presence of clouds limits time series continuity [62]. That is even more problematic with low temporal resolution Earth observation systems.

Indicators such as ST are characterized by high spatial and temporal variability so they require observations both at a very high spatial and at a very high temporal resolution [59]. The low spatial resolution of satellite image products which are associated with ST limits several agricultural applications that require the characterization of the microclimate and the intra-plot variability. Site-specific management of crop pests, as well as management of agricultural inputs and irrigation, requires accurate estimates of crop status and agro-meteorological conditions and characterizations of their intra-plot variability [42]. Several authors are unanimous on the fact that management of diseases and pests, characterized by a high spatial and temporal dynamics, requires specific agro-meteorological information at the field and microclimate scales [67–69]. Matese et al. [70], for example, have shown that the microclimate of vineyards is characterized by high spatial variability (intravignoble and intervignoble) meaning that measurements from meteorological stations located outside of these vineyards do not effectively reflect the microclimate conditions occurring there. Agricultural practices rely increasingly on data acquired at fine scales in order to characterize the spatial and temporal variability of growth factors within the fields in order to improve management of crop diseases and pests and agricultural inputs, and to reduce the costs for producers and the toll on the environment and human health. Airborne remote sensing offers several advantages that can meet this need. Technological advances in recent years in the field of thermal infrared remote sensing led to the development of very high spatial resolution airborne sensors which allow the observation of ST at very fine scales [20]. According to Wood et al. [71], airborne remote sensing is an effective approach to producing accurate information in near real-time to improve the management of agricultural practices (prevention and control of crop diseases and pests, fertilizer application, irrigation, etc.) in a precision farming context. It provides accurate

mapping solutions with flexibility of choice regarding spatial and temporal scales that meet specific needs [42, 72] such as integrated pest management. It was thus demonstrated that images at very high spatial resolution are more appropriate to map riparian vegetation which is characterized by great complexity, great diversity, and spatial variability that manifests itself in very short scales [73]. Wood et al. [71] used airborne images to map the intra-plot variability in wheat fields. Zhang et al. [74] used airborne images to assess the effectiveness of different herbicides in cotton fields. The airborne thermal imagery acquired using infrared thermography cameras was among those used for the detection of water stress [42]. The characterization of the spatial variability of microclimate conditions at fine scales also requires accurate data [42, 68, 69, 75, 76]. This requires the assessment of the uncertainties related to tools and methods used to estimate SMIs.

The aim of our study was to estimate, evaluate uncertainties, and characterize the spatial variability of surface microclimate indicators (amount of vegetation, surface temperature, and surface moisture) derived from airborne infrared thermography and airborne multispectral imaging in the context of prevention and control of vegetable crop diseases and pests.

2. Method

2.1. Study area

The study area is located in the valley of the St. Lawrence River, in the Montérégie West region, in the south of the metropolitan area, and in the southern part of the province of Quebec, Canada (**Figure 1**). The terrain is relatively flat in this study area. Elevations vary between 50

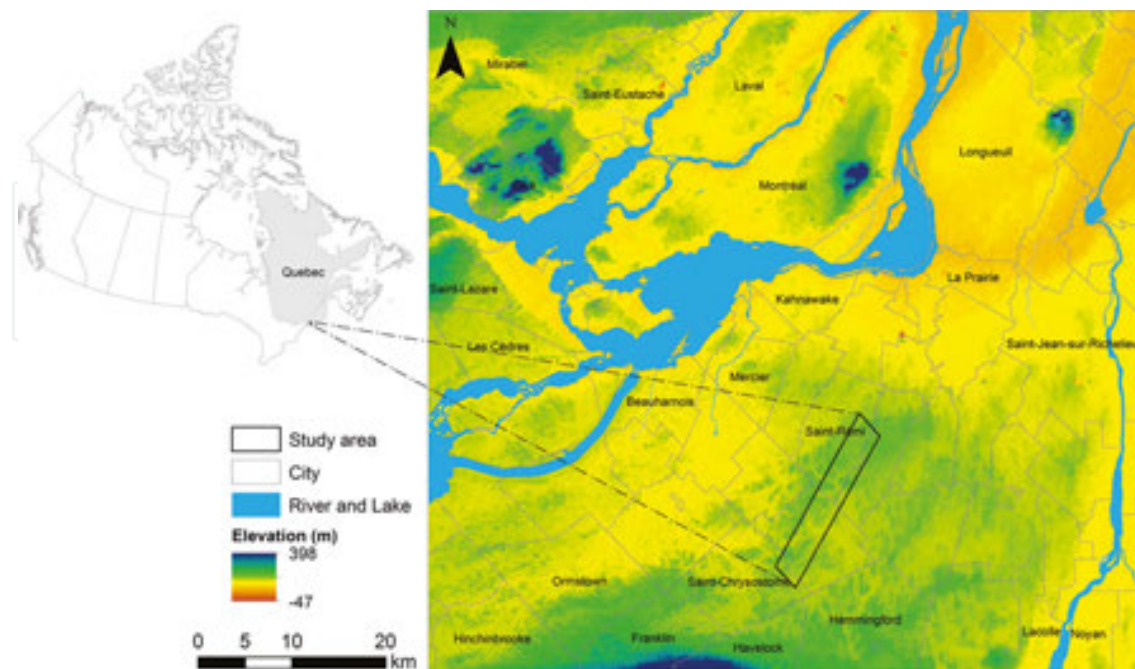


Figure 1. Study area.

and 73 m (average elevation of 60 m), with slopes varying between 0 and 6.14% (average slope of 0.77%) (Canadian Digital Elevation Data [77]). Elevations are higher in the northern half of the study area. Black soil (organic soil) dominates the southern half part, while the northern half is mainly occupied by mineral soil. Forest and wooded areas are mainly located in the south. Agricultural lands are mainly used for vegetable crops (potato, lettuce, onion, carrot, celery, cabbage, etc.) and field crops (soybean and maize). These crops are respectively distributed in the northern part and in the southern part of the study area. Airborne imagery acquisition and in situ measurements were performed on July 14, 2006. Ground recognition was conducted from July 13 to 14, 2006.

2.2. Data acquisition

Figure 2 presents the overall schema of data acquisition and processing.

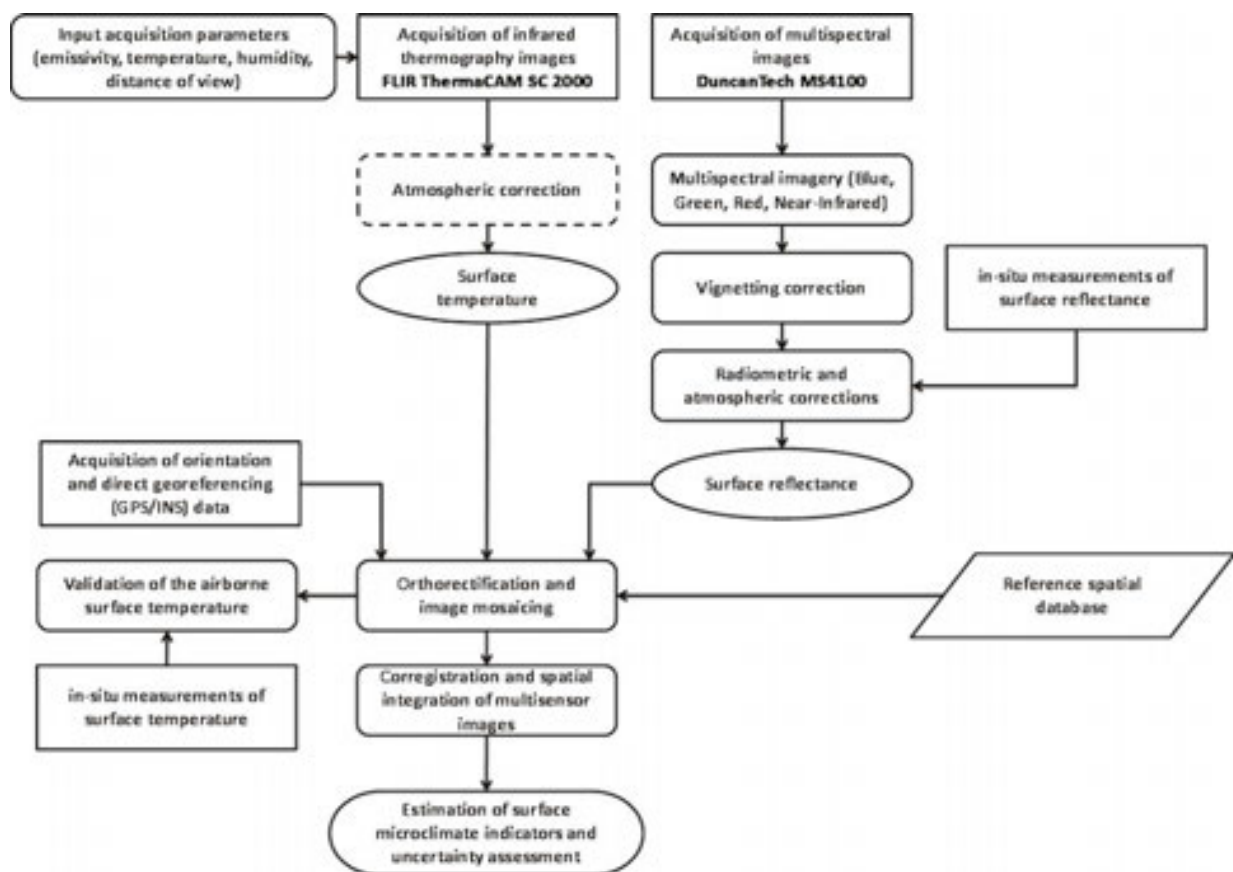


Figure 2. Overall schema of airborne remote sensing data acquisition and processing.

2.2.1. Airborne multispectral imagery and infrared thermography

The MS4100 camera (Duncan Tech, Auburn, CA) was used for the acquisition of airborne multispectral images. It was configured to operate with the spectral bands blue (437–483 nm), green (520–560 nm), red (640–680 nm), and near infrared (767–833). This camera is character-

ized by an image plane of $14.2 \times 8 \text{ mm}^2$, a pixel size of 7.4 microns, an image resolution of 1920×1080 pixels, a focal length of 17 mm, and a field of view of $49^\circ \times 28.6^\circ$ (Duncan Tech 2005).

The acquisition of infrared thermography images was performed with the ThermaCAM SC2000 camera (FLIR Systems Inc., Boston, MA, www.flir.ca). This camera operates in the spectral band of 7.5–13 μm . Its imaging system is a focal plane array (FPA), with an uncooled microbolometer detector of 240×320 pixels. It has a spatial resolution (instantaneous field of view, IFOV) of 1.3 mrad and a field of view (FOV) of $24^\circ \times 18^\circ$, with a minimum view distance of 0.3 m. This latter parameter allows a maximum spatial resolution of $0.4 \times 0.4 \text{ mm}$ (absolute size of each pixel at a distance of 0.3 m). Its thermal resolution or thermal sensitivity is 0.07°C at an ambient temperature of 30°C , with an absolute precision (systematic bias) of $\pm 2^\circ\text{C}$ or $\pm 2\%$.

Images were acquired at a flying height of 1200 m, with 13 flying lines oriented south-west/north-east in the direction of the length. The flying height was determined from an expected spatial resolution of 1.5 m on the infrared thermographic images and an equivalent expected spatial resolution of 0.25 m on the multispectral images. A minimum of 30% lateral (side) overlap was used between images of adjacent flying lines, and a minimum of 60% longitudinal overlap was used between adjacent images of the same flying line. The calculation of these overlaps was based on the technical specifications of the infrared thermography camera. In addition to the remote sensing sensors, the acquisition system also included an integrated Global Positioning System/Inertial Navigation System (GPS/INS), which is a Position and Orientation Solutions for Direct Georeferencing (POS/DG) designed by the Applanix Corporation (Richmond Hill, Ontario, Canada, www.applanix.com). The acquisition system was mounted on an airborne platform carried by a Cessna 310L airplane. Image acquisition took place between 9:15 and 11:06 a.m. Eastern Standard Time, from the western boundary to the eastern boundary of the study area (**Figure 1**).

2.2.2. Field investigation and in-situ measurements

A field reconnaissance was conducted before, during, and after the acquisition of airborne images. It allowed the identification of crop varieties and their phenological stages, the identification of infield problems related to drainage, water and nutrient stress, abiotic damage, stress and damage caused by crop pests and diseases, and yield variation. In situ measurements were carried out for air temperature, relative humidity, surface reflectance, and surface temperature on various sites in the study area during the acquisition of airborne images. These measures were used to correct remote sensing images and to assess the accuracy of estimating agro-meteorological indicators.

2.2.2.1. Air temperature and relative humidity

Air temperature (AT) and relative humidity (RH) were observed from 13 sample points distributed over the study site. These observations were synchronized to the acquisition of airborne images. They were carried out at a height of 1.5 m from the surface using hygrometers (model 6301032 NexxTech, ORBYX electronics, Concord, ON). These instruments

have an absolute accuracy of $\pm 1.8^{\circ}\text{C}$ between 0 and 40°C . A series of nine repeated measurements at 5 s intervals was carried out by sampling point in order to obtain an average measure with a resultant uncertainty of $\pm 0.6^{\circ}\text{C}$. A device was used to protect the hygrometers from wind and direct sunlight. Continuous measurements at 10-min intervals were undertaken during the acquisition of airborne images, using two hygrometers installed at two weather station sites. The comparison of these measures with those acquired by meteorological stations at the same time was used to adjust hygrometer measurements to those of the meteorological stations.

2.2.2.2. *Surface reflectance*

Surface reflectance measurements were performed using a spectroradiometer FieldSpec Pro (ASD Inc., Boulder, CO, www.asdi.com) at two calibration sites (calibration site 1, CS1, and calibration site 2, CS2). On site CS1, reflectance measurements were performed on a white tarpaulin and on green grass. On site CS2, these measures were performed on a water surface (irrigation pond), bare soil (black soil), and on an onion crop surface. Each reflectance measurement was preceded by a calibration of the spectroradiometer using a Spectralon (white reference). Reflectance measurements were carried out simultaneously with the acquisition of airborne images.

2.2.2.3. *Surface temperature*

Surface temperature was measured on the same calibration surfaces used for surface reflectance, during and after the acquisition of airborne images. Infrared thermometer OS643E-LS (Omega, Stamford, CT) was used for these measurements. This instrument measures the temperature using the radiation emitted in the 6–14- μm -wide spectral band (thermal infrared). It has a reading accuracy of $\pm 2\%$, a display resolution of 1°C , and a field of view of 65 mm diameter at 1 m. Surface temperature measurements were performed vertically at a target distance of about 1 m, except for water surface which required an oblique view and a greater distance for reasons of accessibility. Nine measuring points were sampled across each calibration surface. Two types of measurements were performed with the infrared thermometer. The first, called “calibration measurements of the infrared thermometer,” was used to establish the relationship between the measurements of the thermometer and the infrared thermography camera and in order to use the thermometer readings as reference data for the assessment of the uncertainty of the surface temperature derived from the airborne infrared thermography. The calibration measurements of the infrared thermometer were performed at four sites, on a white tarpaulin that served as a reference surface. The geometry of the measurement was configured such that the two sensors covered the same field of view on the tarpaulin. The second type of measurement was used as a validation measure of the estimation of the surface temperature by airborne infrared thermography. These measures were synchronized with the acquired airborne images.

2.3. Data processing

2.3.1. Radiometric and atmospheric corrections

2.3.1.1. Multispectral imagery data

A gradual darkening effect from the center to the edges was found when reading the multispectral images. This phenomenon is known as vignetting [78–80]. It was corrected using the equations proposed by Hasler and Süssstrunk [81].

The empirical line method [82] was used to perform the atmospheric correction of the multispectral images. This method assumes that there is in the image at least one low reflectance target (value close to 0) and one high reflectance target (value close to 1) in each spectral band of the sensor [82–84]. A linear equation that models the relationship between the luminance (or the digital count) and the surface reflectance is set to convert the digital counts in surface reflectance values. Although this approach corrects both radiometric and atmospheric effects and overcomes having to use atmospheric measurements and a radiative transfer model, it does require reflectance measurements on target surfaces with simultaneous image acquisition; this was performed in the present study. The average values of surface reflectance and digital count of the calibration panels were used to establish regression models and derive the equation of the empirical line in each spectral band of the sensor. Three target surfaces were used to determine the empirical line in each spectral band.

2.3.1.2. Infrared thermography data

The infrared camera ThermaCAM SC 2000 is designed for industrial applications and for research and development applications conducted primarily in laboratory. The format of the camera output data does not meet the needs of a geospatial application. The ThermaCAM Researcher software 2001 (FLIR Systems AB, Rinkebyvägen, Danderyd) was used to export the thermography to a MatLab file (.mat). The structure of this file contains information like date and time of data acquisition, object signal, emissivity, temperature, characteristics of the black body and the trigger signal number. From this data structure, the surface temperature matrix was converted into a 32-bit georeferenced Tagged Image File Format (GeoTIFF) image file.

The radiometric calibration and atmospheric correction are internal to the thermal camera. The calibration is performed by measuring digital counts over a blackbody with a known emitted luminance, surface temperature, surface emissivity, and target distance. The data derived from this calibration are used to produce a curve associating digital numbers to luminance values and to establish the relationship between the input luminance of the sensor and the surface temperature of the target. The latter conversion is made using a series of lookup tables (LUTs) stored in the camera. These LUTs establish the relationship between luminance values and blackbody temperatures. When a measurement is made, the system identifies the LUT which is associated with the digital number signal generated and calculates the temperature value related to the measurement. The surface temperature calculated by the camera is based on the law of total radiation [85, 86] by using the infrared radiation emitted by the surface, the

reflected infrared radiation emitted by the surrounding heat sources, and the thermal radiation of the atmosphere Eq. (1).

$$T_{\text{cam}}^4 = \varepsilon\tau ST^4 + (1 - \varepsilon)\tau T_{\text{amb}}^4 + (1 - \tau)T_{\text{atm}}^4 \quad (1)$$

where T_{cam} , input temperature of the camera (K); ε , surface emissivity; τ , transmissivity of the atmosphere; ST , surface temperature (K); T_{amb} , reflected ambient temperature (K); T_{atm} , temperature of the atmosphere (K).

The input parameters used by the thermal camera to solve Eq. (1) were surface emissivity, ambient temperature (temperature of the ambient air from the environment of the object), temperature of the atmosphere (temperature of the air between the object and the camera), the target distance, and the relative humidity of the air. These parameters were provided to the camera before the measurements and were used in post processing to correct the infrared thermography images. The ThermoCAM Researcher software (FLIR Systems, Boston, MA) was used for the acquisition and correction of infrared thermography images. The surface emissivity value was set to 1 in order to calculate an apparent atmospherically corrected blackbody temperature because the acquisition and processing software accepts only one emissivity value by image. However, the surface emissivity varies over the image with the spatial heterogeneity of the observed territory. The surface temperature was subsequently calculated using the apparent blackbody temperature and a surface emissivity map (Section 2.5.2).

2.3.2. Orthorectification and spatial integration

Airborne remote sensing data acquisition was completed with an average of 350 images per flight line for a total of 4500 images per sensor. A conventional aerial triangulation was carried out on subsets of images of different flight lines in order to perform the internal calibration of the sensors and solve the linear and angular eccentricities of the GPS/INS/camera system. A total of 30 images and a minimum of 5 control/tie points per image were used for this calibration. The images used for the calibration are those whose centers coincide with a point that can be defined as a control point (intersection of roads, trails, rivers, or center of irrigation pond, etc.). An algorithm was developed to mark the center of the images to identify those suitable for the calibration. The resolution of eccentricities consisted of comparing the exterior orientation parameters calculated by the conventional aerial triangulation method and those from the GPS/INS system data. Image orthorectification and mosaicking were subsequently performed automatically for each flight line. Then, a mosaic of different image lines was completed. The internal orientation parameters and the values of eccentricity from the calibration, the external orientation parameters from the GPS/INS system data, and a digital elevation model were used as input data in the OrthoEngine module of Geomatica software (PCI Geomatics, Richmond Hill, ON) to perform the orthorectification. Data from the *Base de Données Topographiques du Québec* (BDTQ, topographic database of the province of Quebec,

1/20000) was used as spatial reference to collect control points to assess the overall accuracy of the orthorectified multispectral image and infrared thermography image.

Estimating SMIs by using multisensor data requires a good spatial integration of these data to ensure the linking of homologous pixels from multispectral and thermal images. To achieve this, an average filter of 5×5 pixels and a resampling to the resolution of 5 m were successively applied to the 1.5-m resolution images.

2.4. Image classification

A maximum likelihood supervised classification (MLSC) [87, 88] was performed using airborne multispectral and infrared thermography images to map land use and land cover (LULC). The MLSC was conducted according to different thematic classes including: full cover vegetable crop (FCVC), partial cover vegetable crop (PCVC) (vegetation and visible bare soil), large-scale farming (LSF), hay and grazing land (HGL), organic bare soil (OBS), mineral bare soil (MBS), herbaceous, forest, impervious surface (IS), and water. Field reconnaissance data and the Insured Crop Database (ICDB) of the *Financière agricole du Québec* (www.fadq.qc.ca) were used to collect both training and validation sites. Error statistics like overall accuracy, kappa coefficient, producer accuracy, and user accuracy [89, 90] were used to assess the quality of the classification. The polygons associated with the thematic classes of the classified image were used to evaluate the spatial variability of SMIs according to these classes.

2.5. Estimation of surface microclimate indicators and uncertainty assessment

2.5.1. Vegetation quantity

The normalized difference vegetation index (NDVI) [91] and percent vegetation cover (PVC) were used to express the amount of vegetation and the spatial variability of phenological stages observed in the field. Formulas of NDVI and PVC are, respectively, presented in Eqs. (2) and (3). Vegetation indices (VIs) can be considered as indicators of the amount of vegetation and vegetation biomass [92]. The NDVI is one of the best known and most used of VIs [28, 45, 51, 93], particularly for estimating the amount of vegetation and monitoring crop phenology [34, 46]. The NDVI was estimated using airborne multispectral images, as formulated in Eq. (2). PVC was estimated using the NDVI [94] according to Eq. (3). In a comparative study based on airborne images, Nagler et al. [48] showed that the NDVI gave a better result for estimating PVC, compared to soil-adjusted vegetation index (SAVI) and enhanced vegetation index (EVI). The uncertainty of the NDVI was evaluated by validation using in situ measurements (Eq. (4)). The formulation of the uncertainty of the PVC (Eq. (5)) was based on the law of propagation of uncertainty (LPU) and the combined standard uncertainty assessment approach proposed by the guide to the expression of uncertainty in measurement (GUM) [95].

$$\text{NDVI} = \frac{\rho_{\text{NIR}} - \rho_{\text{R}}}{\rho_{\text{NIR}} + \rho_{\text{R}}} \quad (2)$$

where NDVI, normalized difference vegetation index; Q_R , reflectance of the red band; Q_{NIR} , reflectance of the near infrared band.

$$PVC = \left[\frac{NDVI - NDVI_{\min}}{NDVI_{\max} - NDVI_{\min}} \right]^2 \quad (3)$$

where PVC, percent vegetation cover; $NDVI_{\min}$, NDVI minimum; $NDVI_{\max}$, NDVI maximum.

The parameters $NDVI_{\min}$ and $NDVI_{\max}$, respectively, correspond to the NDVI of bare soil and the NDVI of full vegetation cover. They were estimated using the classified image according to the average NDVI values, respectively, associated with FCVC and PCVC classes.

$$u(NDVI_{\text{airborne}}) = \sqrt{\frac{1}{N-2} \sum_{i=1}^N (NDVI_{\text{airborne}i} - (b + aNDVI_{\text{in situ}i}))^2} \quad (4)$$

where $u(NDVI_{\text{airborne}})$, uncertainty of the NDVI derived from airborne multispectral imagery; $NDVI_{\text{airborne}}$, NDVI derived from airborne multispectral imagery; $NDVI_{\text{in situ}}$, NDVI derived from in situ spectroradiometric measurements; N , number of observations of the pair ($NDVI_{\text{in situ}}$, $NDVI_{\text{airborne}}$); a , slope of the linear regression $NDVI_{\text{in situ}}/NDVI_{\text{airborne}}$; b , intercept of the linear regression $NDVI_{\text{in situ}}/NDVI_{\text{airborne}}$.

$$u(PCV)^2 = 8PCV^2 u(NDVI)^2 \left[\left(\frac{1}{NDVI - NDVI_{\min}} \right)^2 - \left(\frac{1}{NDVI_{\max} - NDVI_{\min}} \right)^2 \right] \quad (5)$$

where $u(PCV)$, PVC estimation uncertainty; $u(NDVI)$, NDVI estimation uncertainty; $NDVI_{\min}$, NDVI minimum threshold corresponding to bare soil; $NDVI_{\max}$, NDVI maximum threshold corresponding to full vegetation cover.

2.5.2. Surface temperature

Surface temperature (ST) was estimated using (Eq. (6)) [96, 97], based on the apparent blackbody temperature derived from the airborne infrared thermography and the surface emissivity model (SEM) estimated according to Sobrino and Raissouni [98]. The largest source of uncertainties in the estimation of the ST derived from airborne infrared thermography are related to the input parameters of the temperature model (Eq. (1)). They include surface emissivity model, ambient temperature, temperature of the atmosphere, relative humidity of the air, viewing distance, error induced by the ambient infrared radiation reflected by the surface, estimation error of the transmissivity of the atmosphere, and atmospheric radiation [99]. The surface emissivity model is the most important source of uncertainty [99, 100]. Orthorectification and image coregistration and mosaicking are other non-negligible sources

of uncertainty. Considering all these uncertainty components, the formal assessment of the resultant uncertainty of the ST derived from airborne infrared thermography (ST_{airborne}) using analytical methods such as LPU is not easy to achieve. The uncertainty of the ST_{airborne} was estimated by validation, as an experimental uncertainty combining all the above uncertainty components. The assessment of the experimental uncertainty was performed using in situ measurements carried out by infrared thermometry ($ST_{\text{in situ}}$) (Eq. (7)).

$$ST = \frac{T_b}{\epsilon_s^{\frac{1}{4}}} \quad (6)$$

where ST, surface temperature (K); T_b , apparent blackbody temperature (K); ϵ_s , surface emissivity (0, 1).

$$u(ST_{\text{airborne}}) = \sqrt{\frac{1}{N-2} \sum_{i=1}^N (ST_{\text{airborne}i} - (b + aST_{\text{in situ}i}))^2} \quad (7)$$

where $u(ST_{\text{airborne}})$, uncertainty of the surface temperature derived from airborne infrared thermography (K); ST_{airborne} , surface temperature derived from airborne infrared thermography (K); $ST_{\text{in situ}}$, surface temperature derived from in situ infrared thermometry (K); N , number of observations of the pair ($ST_{\text{in situ}}$, ST_{airborne}); a , slope of the linear regression $ST_{\text{in situ}}/ST_{\text{airborne}}$; b , intercept of the linear regression $ST_{\text{in situ}}/ST_{\text{airborne}}$.

2.5.3. Surface humidity

Surface humidity (SH) was estimated using the temperature/vegetation dryness index (TVDI) proposed by Sandholt et al. [101]. This index is based on the principle that the direct relationship between soil moisture and ST is not easy to assess. However, soil moisture is an important factor in the spatial and temporal variability of ST. It influences ST via evapotranspiration and the thermal properties of the surface [101]. Also, the status of the vegetation cover is a function of soil water content. Thus, the curve relating ST and NDVI, commonly known as the ST/NDVI space, allows the assessment of the moisture conditions of the surface and the estimation of soil water status [24, 34, 56, 101–105]. For a given site, the point cloud of the relationship TS/NDVI defines a trapezoidal space. This space is a set of isolines representing different states of surface moisture [105]. Its left vertical edge represents bare soil, from a dry state corresponding to an absence of evapotranspiration (E_{null}), to a wet state corresponding to a maximum of evapotranspiration (E_{max}). The horizontal line of the lower limit of the trapezoid defines the wet edge with minimum values of ST (ST_{min}). It reflects the increase of the green vegetation amount along the x axis (increasing NDVI). The slope of the line representing the upper limit of the trapezoid is defined as the dry edge with maximum values of ST (ST_{max}). Eq. (8) shows the formulation of the TVDI, which varies between 0 and 1. A value of 1 corresponds

to dry conditions and is associated with limited water availability. The value 0 corresponds to maximum evapotranspiration and unlimited water availability.

$$\text{TVDI} = \frac{ST - ST_{\min}}{ST_{\max} - ST_{\min}} \quad (8)$$

where ST , surface temperature (K); ST_{\min} , line of the wet edge defining the minimum value of ST (K); ST_{\max} , line of the dry edge defining the maximum value of ST (K).

The line of the dry edge is defined as follows:

$$ST_{\max} = a + b \times \text{NDVI} \quad (9)$$

The parameters a and b are the coefficients of the linear regression ST/NDVI determined using the points defining the upper limit of the ST/NDVI space.

The calculation of TVDI is based on the presence of pixels of full vegetation cover, pixels of bare soil, and mixed pixels of vegetation and bare soil in the ST/NDVI space. The classified image was used to identify those pixels in order to compute the point cloud of the ST/NDVI space and to estimate the edge lines needed for the calculation of the TVDI.

The uncertainty of the TVDI was formulated in Eq. (10) on the basis of the LPU [95].

$$u(\text{TVDI})^2 = \text{TVDI}^2 \left[\left(\frac{u(ST)}{ST - ST_{\min}} \right)^2 + \left(\frac{u(ST_{\max})}{ST_{\max} - ST_{\min}} \right)^2 + \left(\frac{1}{ST_{\max} - ST_{\min}} + \frac{1}{ST - ST_{\min}} \right)^2 u(ST_{\min})^2 \right] \quad (10)$$

where $u(\text{TVDI})$, uncertainty of the temperature/vegetation dryness index; $u(ST)$, uncertainty of the surface temperature (K); $u(ST_{\max})$, uncertainty of the surface temperature related to the dry edge of the ST/NDVI space (K); $u(ST_{\min})$, uncertainty of the surface temperature related to the wet edge of the ST/NDVI space (K).

The uncertainty $u(ST)$ is equal to $u(ST_{\text{airborne}})$ (Eq. (7)). Uncertainties $u(ST_{\max})$ and $u(ST_{\min})$ were estimated using the variance of the residuals of the regression lines, respectively, associated with the upper edge (Eq. (11)) and the lower edge (Eq. (12)) of the ST/NDVI space.

$$u(ST_{\max}) = \sqrt{\frac{1}{N_{\text{pls}} - 2} \sum_{i=1}^{N_{\text{pls}}} (ST_{\max i} - (a + b \times \text{NDVI}_i))^2} \quad (11)$$

where $u(ST_{\max})$, uncertainty of the surface temperature related to the dry edge of the ST/NDVI space (K); ST_{\max} , surface temperature of the dry edge of the ST/NDVI space (K); NDVI, normalized difference vegetation index (-1, 1); a and b , intercept and slope of the line of the dry edge of the ST/NDVI space; N_{pls} , number of pixels used to define the line of the dry edge of the ST/NDVI space.

$$u(ST_{\min}) = \sqrt{\frac{1}{N_{\text{pli}} - 1} \sum_{i=1}^{N_{\text{pli}}} (ST_{\min i} - \overline{ST}_{\min})^2} \quad (12)$$

where $u(ST_{\min})$, uncertainty of the surface temperature related to the wet edge of the ST/NDVI space (K); ST_{\min} , surface temperature related to the wet edge of the ST/NDVI space (K); \overline{ST}_{\min} , average surface temperature of the wet edge of the ST/NDVI space (K); N_{pli} = number of pixels used to define the line of the wet edge of the ST/NDVI space.

The TVDI estimated from airborne images was validated using in situ measurements of AT and HR, as surface moisture was not measured during the field campaign. This validation is based on the assumption that conditions of high surface moisture are locally associated with lower values of AT and higher values of HR. Conversely, dry surface conditions are locally associated with higher AT values and lower HR values.

3. Results

3.1. Land use and land cover

Airborne multispectral imaging and infrared thermography helped achieve good classification results in the study area. Overall accuracy and kappa coefficient of the supervised classification were, respectively, 84.87% and 0.85. The classified image showed that agricultural surfaces represent the main LULC of the study area (53.25%). The proportion of this area occupied by the other LULC themes is 28.82% for forests, 11.66% for hay and grazing land, 2.63% for impervious surfaces, and 0.28% for water (**Figure 3**). Vegetable crops and large-scale farming are the main components of agricultural surfaces. They occupy 23.50 and 17.58%, respectively, of the study area. The proximity of vegetable crops with organic bare soil (OBS) shows that they are mainly grown on this type of soil. The presence of OBS on vegetable crop fields denotes the high variability that could characterize the microclimate of these environments.

3.2. Vegetation quantity

The NDVI derived from airborne multispectral imaging ($NDVI_{\text{aero}}$) varies in the study area between -0.73 and 0.84 (**Figure 4**), with an average value of 0.34 and a standard deviation of ± 0.31 . It is strongly correlated with the NDVI derived from in situ observations ($r = 0.994$; $p = 0.006$) (**Figure 5**). Uncertainty and bias of the $NDVI_{\text{aero}}$ based on in situ observations, are, respectively, ± 0.045 and -0.118. On average, the $NDVI_{\text{aero}}$ underestimates the NDVI values by

about 0.118. The NDVI map shows three major classes of LULC in the study area (**Figure 4**). In the first group, IS, dry crop residues, and MBS have NDVI values less than 0. In the second group, water, OBS, and PCVC have NDVI values between 0 and 0.33. In this category, OBS is characterized by NDVI values between 0 and 0.29, with an average value of 0.10 and a standard deviation of ± 0.045 . The third group includes forest and FCVC surfaces, which are characterized by the highest values of NDVI (NDVI mean = 0.60).

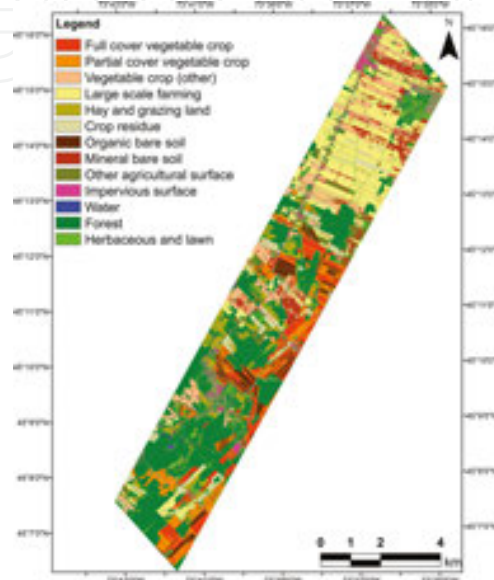


Figure 3. Classification of the land use and land cover using airborne multispectral imagery and infrared thermography.

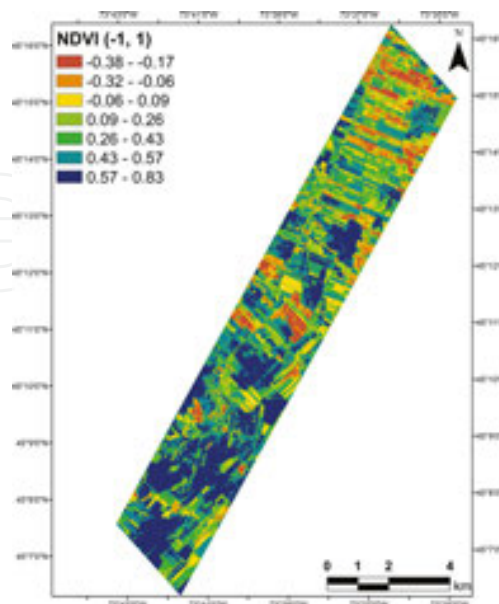


Figure 4. Variation of the normalized difference vegetation index (NDVI) over the study area.

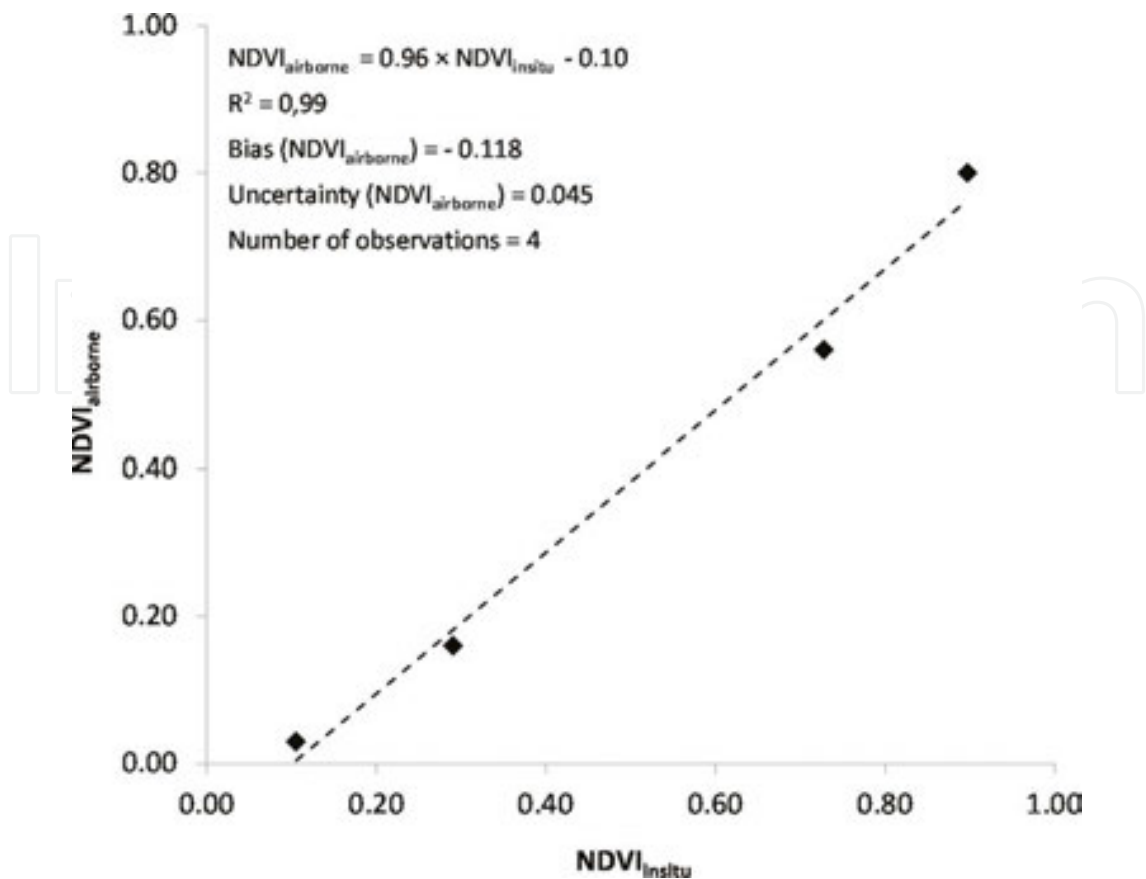


Figure 5. Validation and uncertainty assessment of the NDVI derived from airborne multispectral imagery with in-situ observations.

Average values of NDVI associated with OBS (0.10) and full vegetation cover (0.60) were, respectively, used as minimum and maximum values of NDVI for the estimation of PVC (Eq. (3)). **Figure 6** shows the map of the variation of PVC over the study area. It varies between 0 and 1, with an average value of 0.48 and a standard deviation of ± 0.42 . Its resultant uncertainty varies between 0 and ± 0.365 over the study area (**Figure 7**). The variation of PVC and its resultant uncertainty according to NDVI is illustrated by **Figure 8**. PVC uncertainty increases with NDVI values. Thus, highest PVC uncertainties are observed on areas with greater vegetation cover and lowest PVC uncertainties are observed on areas with smaller vegetation cover (**Figure 8**). The average value of PVC on FCVC surfaces is 0.70, with an average uncertainty of ± 0.279 , while PCVC surfaces have an average value of 0.48 PVC, with an average uncertainty of ± 0.215 . Comparatively, forest cover is characterized by an average value equal to 0.90 PVC, with an average uncertainty of ± 0.338 . PVC is characterized by a lower spatial variability compared to NDVI, because all NDVI values less than or equal to 0.10 have a PVC value equal to 0 and, all NDVI values greater than or equal to 0.60 have a PVC value of 1. However, the spatial dynamics of agricultural surfaces, ranging from bare soil (PCV = 0) to complete vegetation cover (PCV = 1), is best described by PVC rather than NDVI. To illustrate this, **Figure 9** show the variation of NDVI and PVC values on potato crop fields in different phenological stages.

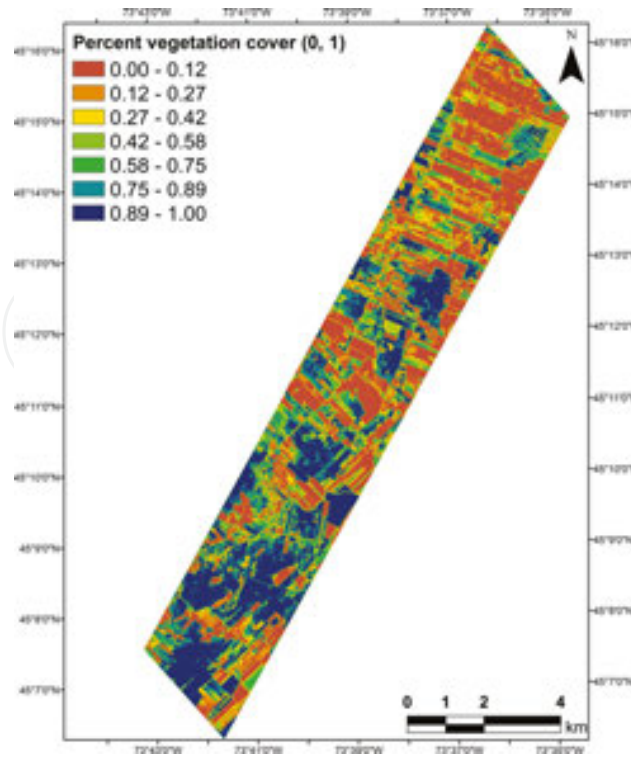


Figure 6. Variation of the percent vegetation cover (PVC) over the study area.

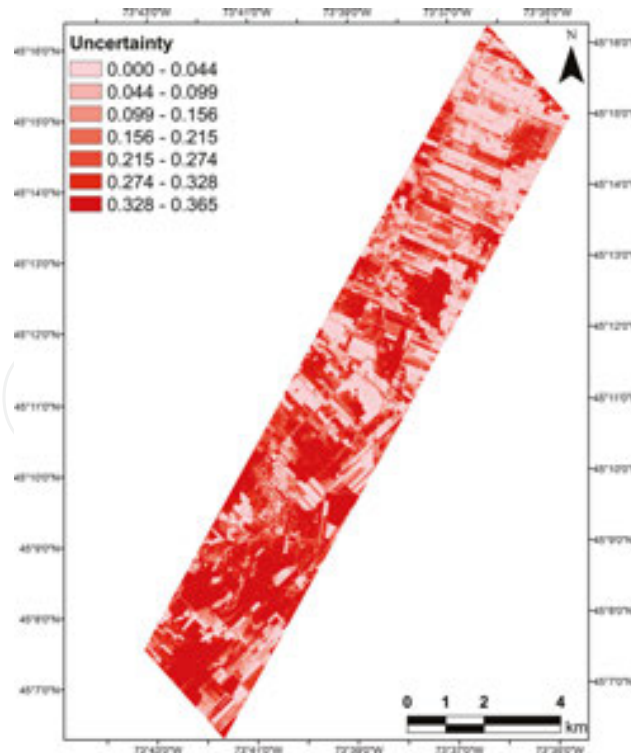


Figure 7. Variation of the uncertainty of the percent vegetation cover (PVC) over the study area.

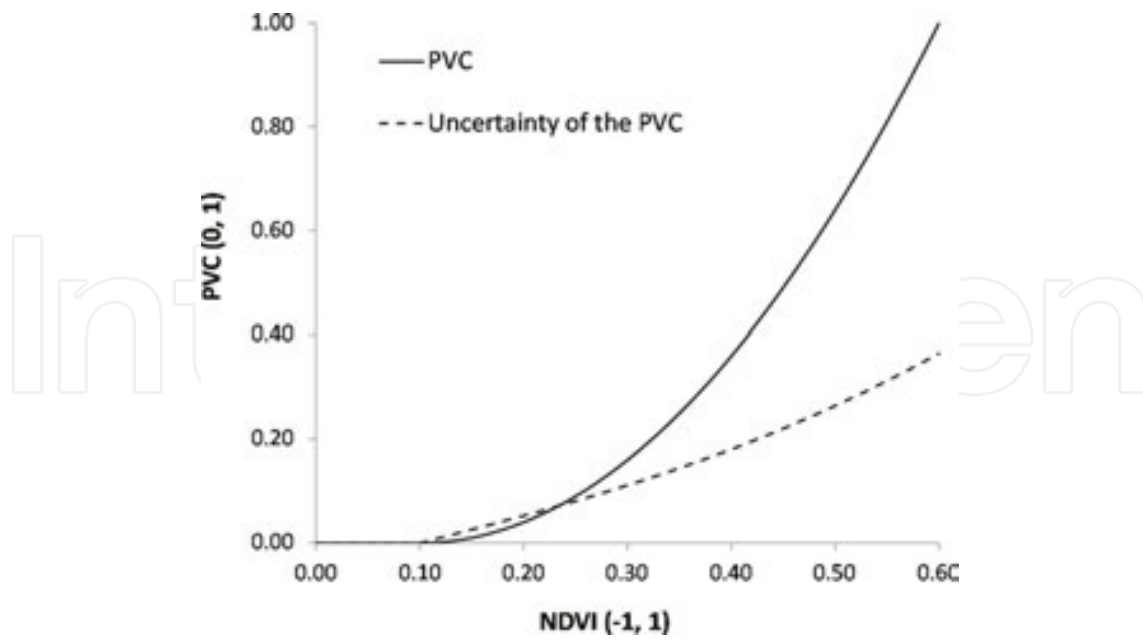


Figure 8. Variation of the percent vegetation cover (PVC) and its uncertainty according to the normalized difference vegetation index (NDVI).

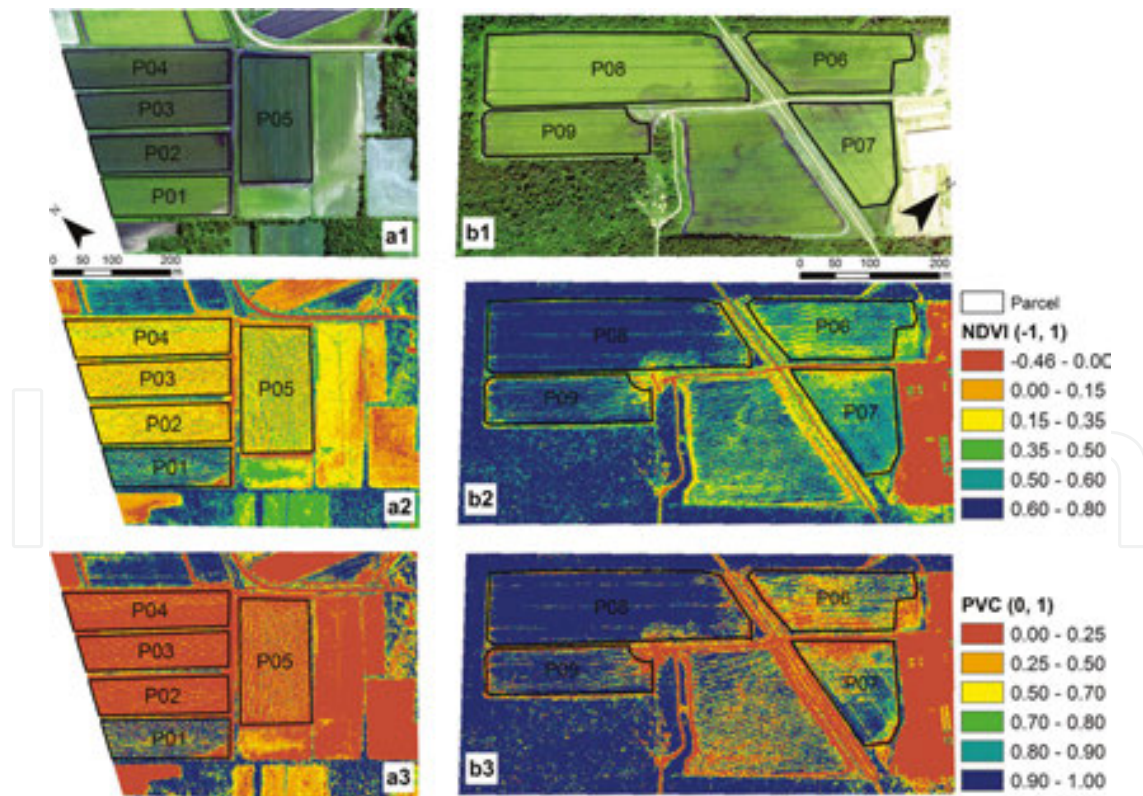


Figure 9. Variation of the normalized difference vegetation index (NDVI) and the percent vegetation cover (PVC) over potato crops at different phenological stages.

3.3. Surface temperature

Surface temperature estimated by airborne infrared thermography (ST_{airborne}) demonstrates a very high thermal spatial variability over the study area (**Figure 10**). This variability occurs both at the intra-plot and local scales. In the period of airborne data acquisition (09:10–11:00 am) and across the study area, the ST_{airborne} varies from 290 to 331 K, with an average value of 300.60 K ($SD = \pm 3.42$ K). This represents a spatiotemporal variation of more than 40 K over an area of 56 km² and a period of about 2 h. The correlation between ST_{airborne} and $ST_{\text{in situ}}$ is very high ($r = 0.99$; $p = 0.010$) (**Figure 11**). The experimental uncertainty and the bias of the ST_{airborne} compared to in situ observations are, respectively, 0.73 and ± 1.42 K.

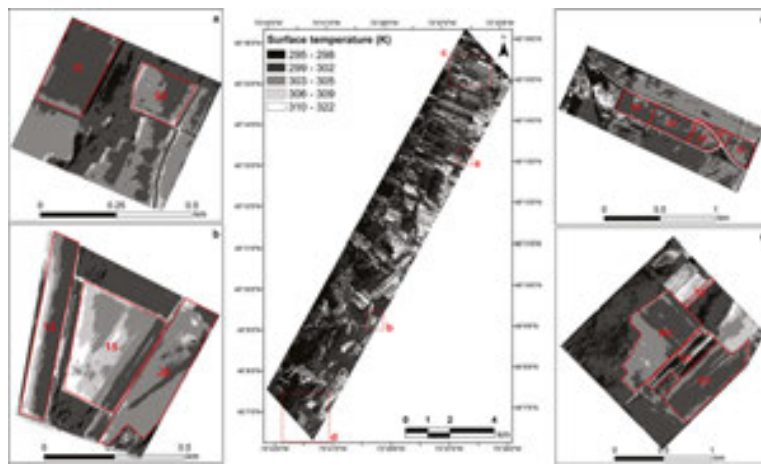


Figure 10. Variation of the surface temperature (ST) over the study area: (a) ST variation according to soil type, (b) ST variation according to soil quality, (c) ST variation on crop surfaces according to soil drainage, and (d) ST variation according to crop varieties and phenological stages.

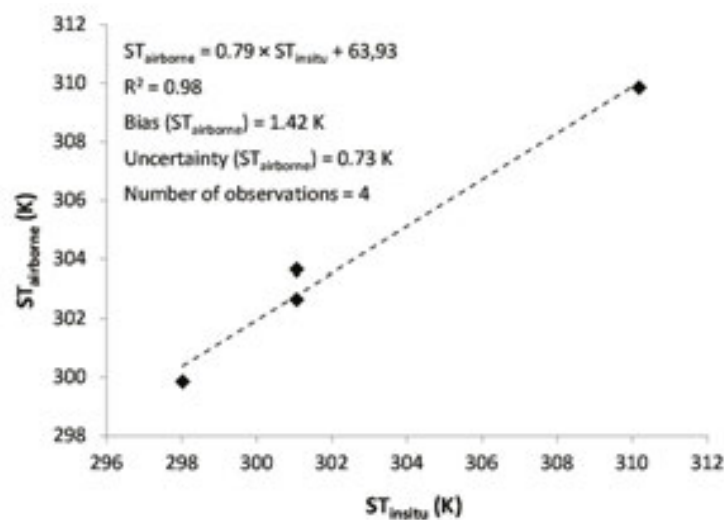


Figure 11. Validation and uncertainty assessment of the surface temperature (ST) derived from airborne infrared thermography with in situ observations.

Table 1 shows the variations of ST_{airborne} on various classes of LULC. Highest temperature values and highest temperature variations are observed on impervious surfaces ($ST_{\text{mean}} = 309.99$ K, $SD = \pm 5.12$ K, $ST_{\text{max}} - ST_{\text{min}} = 39.5$ K). Lowest temperature values and lowest temperature variations are observed on surface waters ($ST_{\text{mean}} = 296.67$ K, $SD = \pm 0.74$ K). The standard deviation of the temperature associated with this class is very close to the uncertainty of ST_{airborne} . Among vegetation areas, forests present the lowest temperature values and the lowest temperature variations ($ST_{\text{mean}} = 297.87$ K, $SD = \pm 0.97$ K). Surface temperature values and variations of full cover vegetable crops ($ST_{\text{mean}} = 298.91$ K, $SD = \pm 1.43$ K) are close to those of large scale farming ($ST_{\text{mean}} = 298.01$ K; $SD = \pm 1.57$ K), while ST values and variations of partial cover vegetable crops ($ST_{\text{mean}} = 302.22$ K; $SD = \pm 2.60$ K) are closer to those of hay and grazing surfaces ($ST_{\text{mean}} = 302.01$ K; $SD = \pm 2.55$ K). Temperature variation reached 8 K on full cover vegetable crop surfaces, while ST varied over 17 K on partial cover vegetable crops. These large variations are mainly due to soil temperature. ST values are on average higher and vary much more on organic bare soil ($ST_{\text{mean}} = 307.36$ K; $SD = \pm 3.87$ K) than on mineral bare soil ($ST_{\text{mean}} = 304.65$ K; $SD = \pm 2.52$ K). The variations of ST on organic bare soil reached 20.33 K and the difference between the ST of vegetable crops and the ST of organic bare soil reached 21.44 K. This very high variation of ST on organic bare soil may be due to water status and the high spatial and temporal dynamics of the temperature of this type of surface.

	Surface temperature (K)			
	Minimum	Maximum	Mean	Standard deviation
Impervious surface	291.66	331.16	309.88	5.12
Water	293.73	298.91	296.67	0.74
Forest	294.84	303.36	297.87	0.97
Hay and grazing land	295.75	311.32	302.01	2.55
Full cover vegetable crop	296.25	304.33	298.91	1.43
Partial cover vegetable crop	297.13	314.16	302.22	2.6
Large scale farming	294.92	305.7	298.01	1.57
Mineral bare soil	297.45	314.31	304.65	2.52
Organic bare soil	297.36	317.69	307.36	3.87

Table 1. Variation of the surface temperature derived from airborne infrared thermography in the study area according to land use and land cover.

Field survey and in situ observations show that intra-field variability of ST_{airborne} observed in vegetable crops are associated with spatial patterns which are related to

- Topographic variation
- Variation of soil type (organic versus mineral soil)
- Different states of organic matter in black soil crops (decomposed soil, not decomposed soil, loam)

- Soil drainage problems in certain areas of the field
- Bare soil versus vegetation areas
- Presence of different crop varieties on the same plot
- Variation of crop phenology on the same field due to different planting dates of crop units
- Water and mineral stress
- Abiotic damage due to phenomena like strong wind, heavy rain, heat stress, farm machinery, and pesticides
- Stress and biotic damage caused by disease and pests
- Proximity to windbreaks (windproof effect)
- Yield variation

The study area is mainly composed of organic and mineral soil. Organic soils are mostly located in the south part which was formerly covered by lakes. Hence, a strong relationship between land elevation and soil type in the area. The values of ST are higher on organic soil compared to mineral soil. Loam soils are sometime present on organic soil fields. **Figure 10a** shows a strong variability of ST between a loam zone (higher values of ST) and an organic soil zone (lower ST values) on field 53. On some fields, the organic soil is not well decomposed. Its nutritional quality is reduced. This causes growth problems and gives rise to a high intra-field variability of ST, which is the case with field 15 on which is grown Chinese cabbage (**Figure 10b**). Poor drainage and flooding caused by underground tanks, for example, can hamper crop growth and lead to a strong spatial variability of ST due to lower vegetation cover in the problematic areas of the field. **Figure 10c** shows a maize crop field affected by poor soil drainage. The temperatures are higher on the problematic areas of the field due to lower vegetation cover.

Intra-field variation from bare soil to full vegetation cover is associated with the highest temperature variabilities observed on the fields (**Figure 10d**, field G3). ST values are much higher on bare soil than on full cover vegetable crops. **Figure 10d** shows temperature variations above 14 K on field G3, which is a mix of bare soil and vegetation. Different crop varieties are characterized by varying phenology, canopy structure, and planting dates. This causes a spatial variability of ST. **Figure 10d** shows temperature variations between lettuce, celery, and potato crops. Subdivision of fields according to different planting dates results in a variation of phenological stages within the same crop variety, hence a variation of percent vegetation cover and ST within the field. Spatial variability of ST on field M3 (celery crop) (**Figure 10d**) is primarily a function of growth stages associated with different planting dates. The lowest temperatures are those of the vegetation cover of the most mature plants. While higher temperatures are associated with younger plants, which are characterized by a lower percent vegetation cover. Spatial variability of ST on crop surfaces are related not only to the variability of soil and crop varieties but also to several other agrometeorological factors such as soil moisture, nutrient and water stress, abiotic damage by weather conditions or cultural practices, and damage caused by pests. Thus, a high spatial variability of ST over a field or crop unit

may indicate a crop growth problem and therefore reflect variability in yield. Temperature variability of the field presented at **Figure 10c** is strongly correlated with yield maps (not presented here—yield maps were shown by the farmer).

3.4. Surface humidity

3.4.1. Lines of dry and wet edges of the TS/NDVI space and their uncertainties

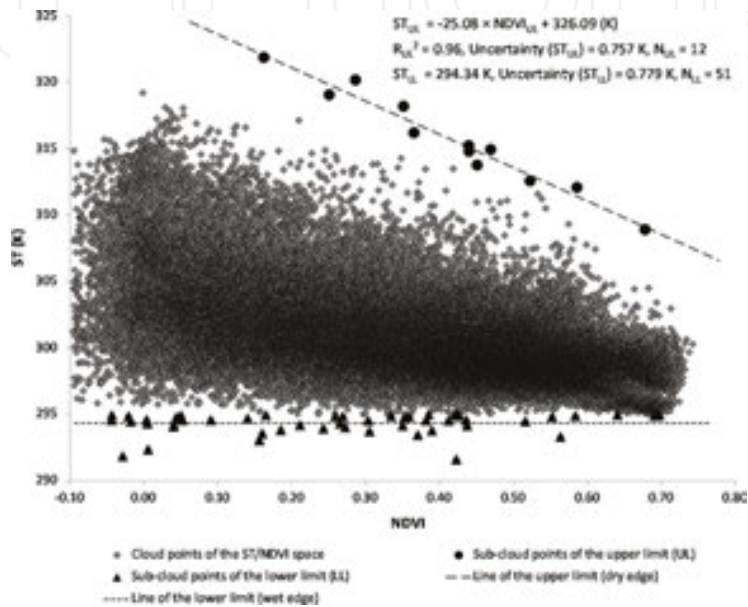


Figure 12. Cloud points of the ST/NDVI space and estimation of dry edge and wet edge lines.

Cloud points of the ST/NDVI space established with airborne infrared thermography and airborne multispectral images describe a trapezoidal area where the upper edge is associated with the highest dry conditions and the lower edge is associated with the highest moisture conditions (**Figure 12**). The cloud points of the upper edge were used to establish the equation of the dry limit ($ST = -25.08 \times NDVI + 326.09$ (K)) with an uncertainty of ± 0.757 K, and the cloud points of the lower edge was used to establish the equation of the wet limit ($ST = 291.61$ K) with an uncertainty of ± 0.779 K. Both uncertainty values are close to the one of ST_{airborne} . The points of the wet limit are mainly located on the western edge of the study area, while a large majority of the points of the dry limits are located on the eastern boundary. The western boundary is the location of the first flight lines' images, acquired in the morning during the period of the lowest ST values. The points of the wet limit are located on vegetation surfaces and on bare soil with low ST values. The eastern boundary is the location of the last flight lines' images, acquired late in the morning when ST values are higher.

3.4.2. Surface moisture variability and uncertainty components of the TVDI

The map of the TVDI confirms that the wetter surfaces are located on the western side of the study area and the driest surfaces are located on the eastern part (**Figure 13**). There are

however, some drought islands (TVDI > 0.50) in the wetter zone and some moisture islands (TVDI < 0.30) in the driest zones. Among the drought islands, there are hay, organic bare soil, and low cover vegetable crops on organic soil (PCV < 0.25). Organic bare soil, full cover vegetable crops, and partial cover vegetable crops are among the moisture islands observed in the driest areas. Over the study area and the period of observation, the TVDI ranges between 0 and 1, with a mean value of 0.35 (SD = ± 0.097). Its uncertainty varies between ± 0.021 and ± 0.126 (Figure 14), with an average value of ± 0.055 (SD = ± 0.016). The histogram of the uncertainty of the TVDI shows three peaks around the values ± 0.033 , ± 0.040 , and ± 0.068 (Figure 15). The map of the uncertainty confirms these three peaks which are associated with three types of surfaces (Figure 14). The first type corresponds to surfaces of low values of NDVI such as mineral bare soil, hay, and grazing lands. The second type also corresponds to surfaces of low NDVI values such as organic bare soil and low cover vegetable crops on organic soil. Areas with a high percent vegetation cover, dominated by forests and full cover crops, compose the third type of surface on which higher values of uncertainty are observed (Figure 14). This shows that the uncertainty of the TVDI increases with the NDVI (Figure 16). Figures 17 and 18 show that this uncertainty also increases when the ST or the temperature of the dry limit (ST_{max}) are near the temperature of the wet limit (TS_{min}). However, this situation generally corresponds to a high vegetation cover with low ST values, therefore a tendency to observe low values of TVDI and higher surface moisture values. These conditions converge toward the wet limit (Figure 19).

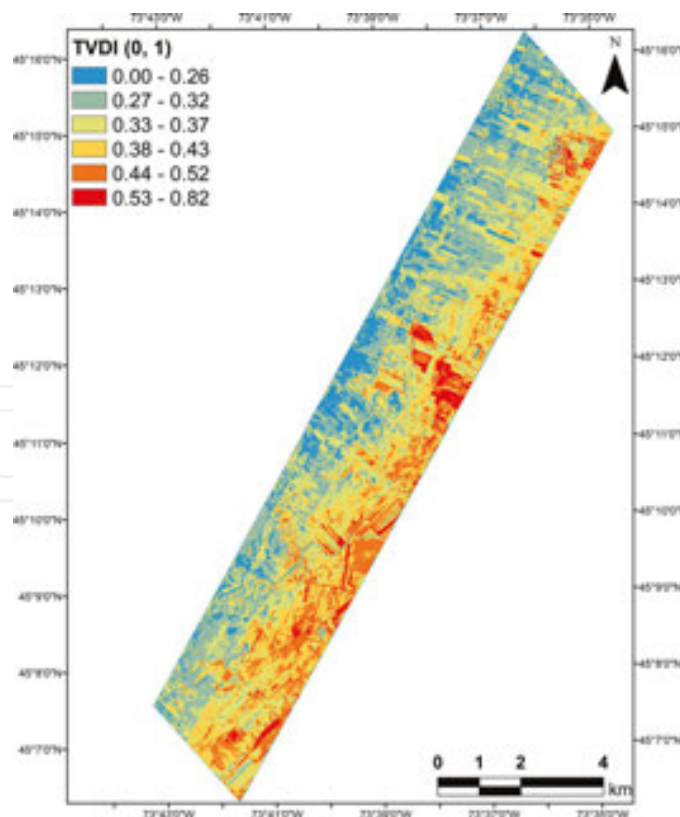


Figure 13. Variation of the temperature/vegetation dryness index (TVDI) over the study area.

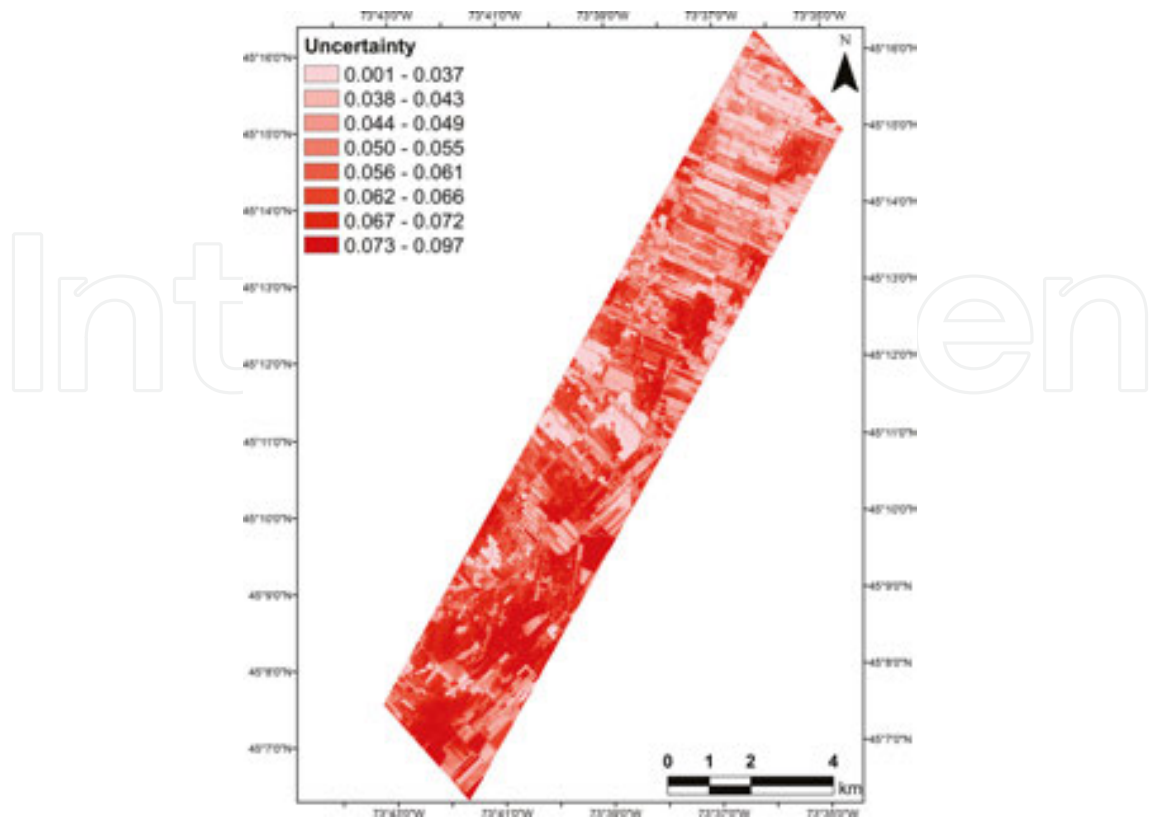


Figure 14. Variation of the uncertainty of the temperature/vegetation dryness index (TVDI) over the study area.

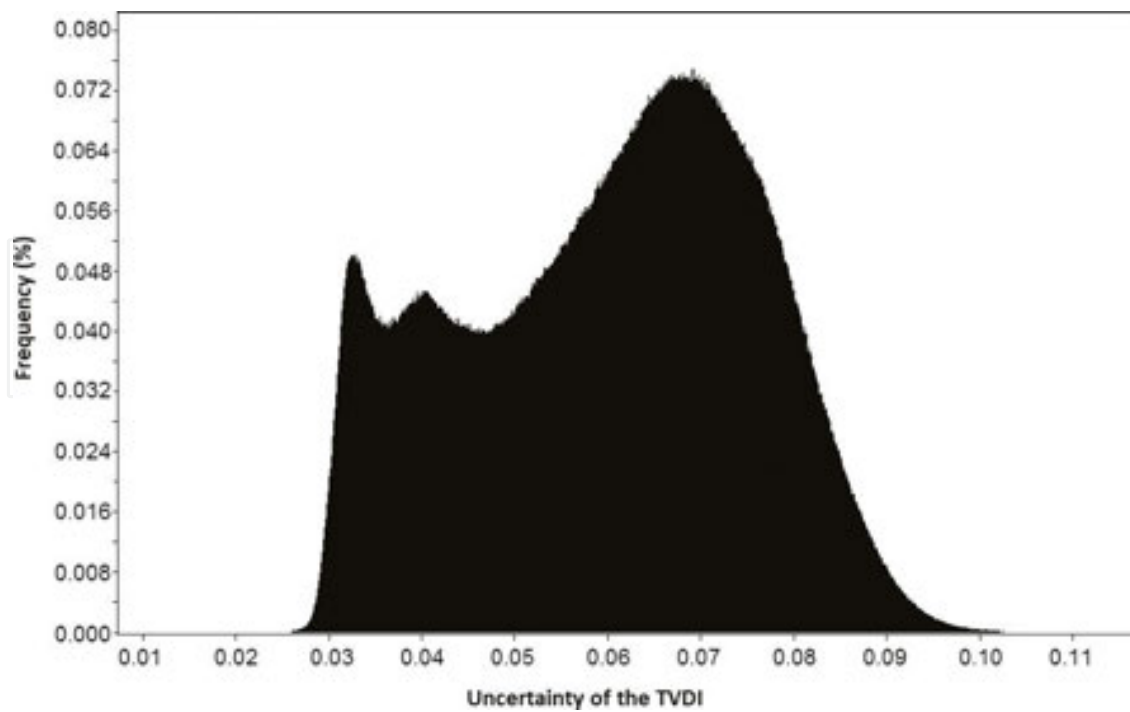


Figure 15. Histogram of the uncertainty of the temperature/vegetation dryness index (TVDI) over the study area.

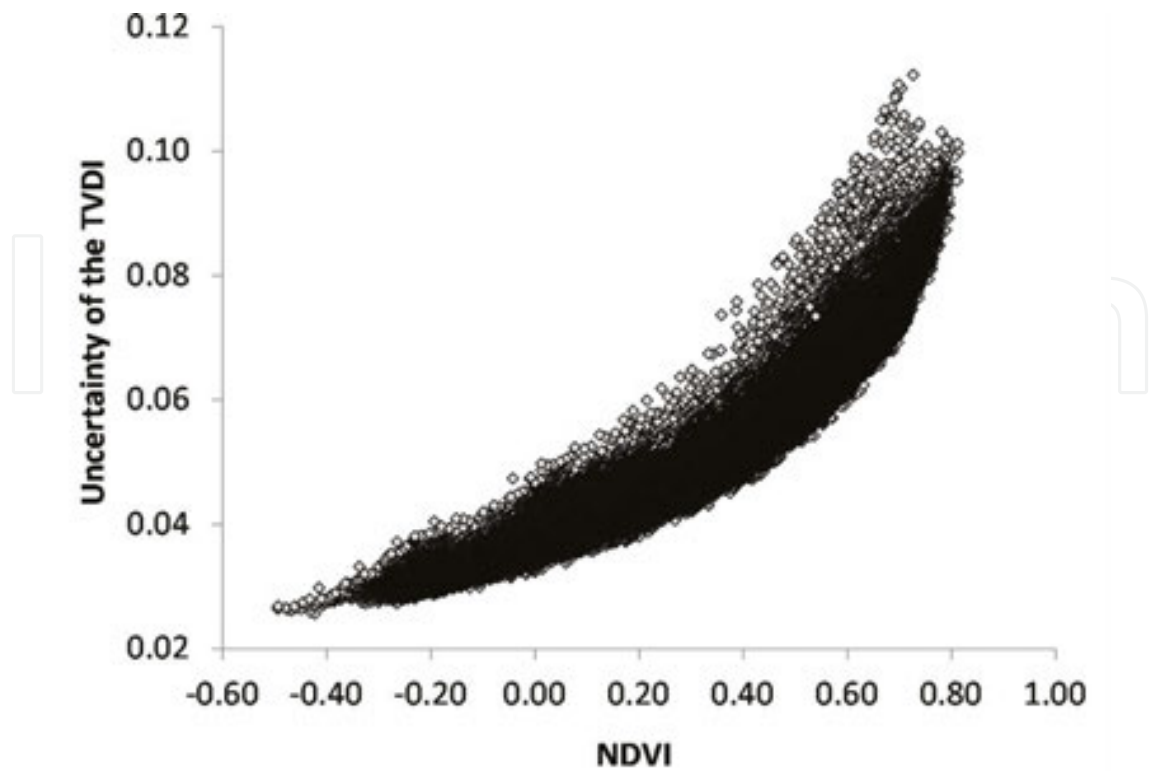


Figure 16. Variation of the uncertainty of the temperature/vegetation dryness index (TVDI) according to the normalized difference vegetation index (NDVI).

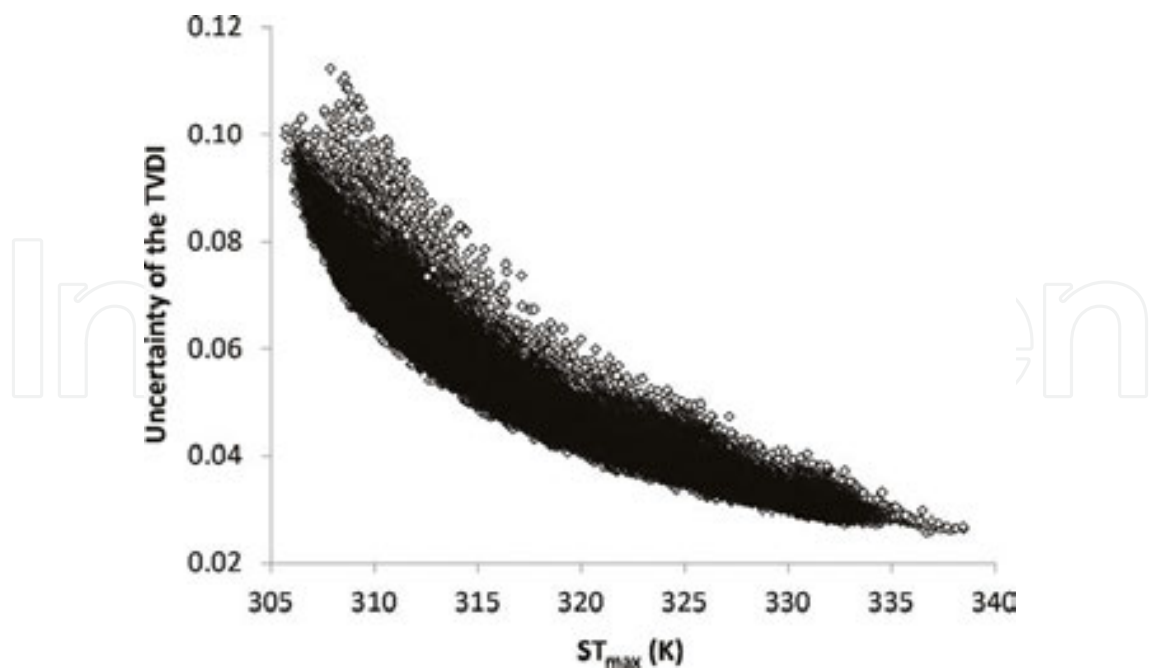


Figure 17. Variation of the uncertainty of the temperature/vegetation dryness index (TVDI) according to the surface temperature of the dry edge (ST_{max}).

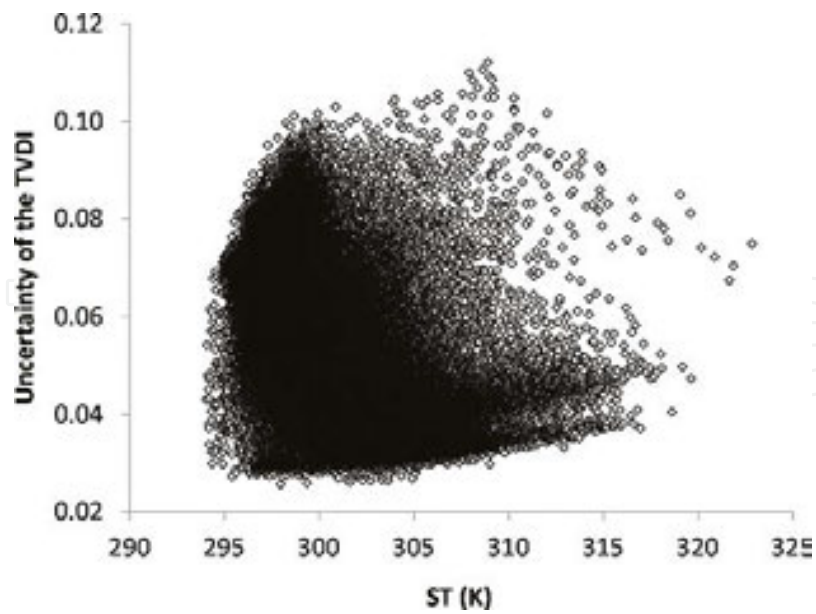


Figure 18. Variation of the uncertainty of the temperature/vegetation dryness index (TVDI) according to the surface temperature (ST).

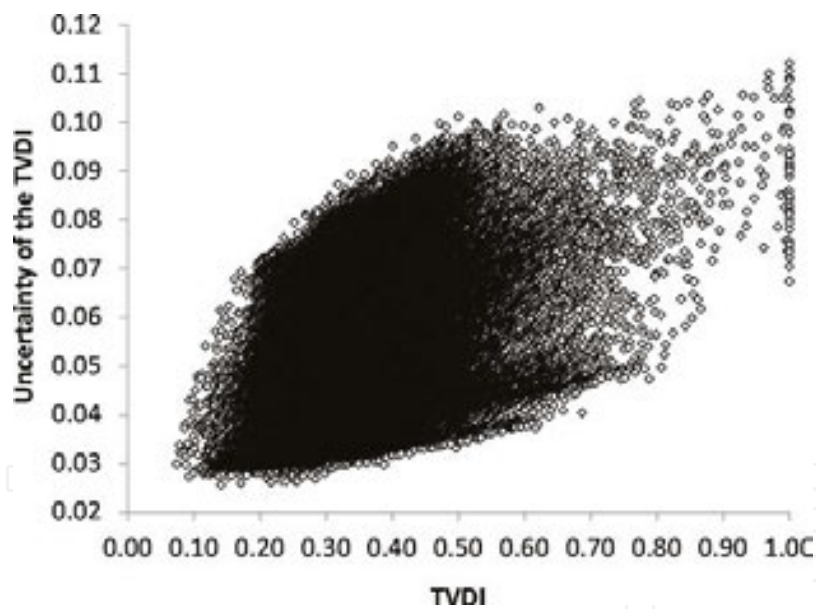


Figure 19. Variation of the uncertainty of the temperature/vegetation dryness index (TVDI) according to the TVDI.

3.4.3. Spatial variability of the TVDI on agricultural surfaces

The TVDI varies between 0.20 and 0.70 across full cover vegetable crop surfaces, with an average value of 0.39 ($SD = \pm 0.076$) and an average uncertainty of ± 0.067 ($SD = \pm 0.006$). This shows that the surface moisture is much lower in some agricultural parcels compared to others. However, full cover vegetable crops are on average wet surfaces rather than dry. This trend

is also observed on partial cover vegetable crop surfaces where the TVDI varies between 0.15 and 0.93, with an average value of 0.44 (SD = ± 0.093) and an average uncertainty value of ± 0.058 (SD = ± 0.011). Much drier surfaces are observed on partial cover vegetable crops compared to full cover vegetable crops. On average, surface moisture was higher on large-scale crops compared to vegetable crops. The TVDI values of the first ones vary from 0.14 to 0.83, with an average value of 0.31 (SD = ± 0.065) and an average uncertainty value of ± 0.064 (SD = ± 0.009). Surface moisture of organic bare soils is highly variable (TVDI: AV = 0.48, SD = ± 0.116), with very wet surfaces (TVDI < 0.25) and very dry surfaces (TVDI > 0.75), while mineral bare soil surfaces are wetter on average (TVDI: AV = 0.33, SD = ± 0.063).

3.4.4. Relationship between the TVDI and in situ observations of air temperature and relative humidity

The relationship between the TVDI and in situ observations shows that it is highly correlated with air temperature ($r = 0.88$, $p = 0.004$, **Figure 20**). However, it does not present a correlation with relative humidity ($r = 0.09$; $p = 0.826$). The correlation between the TVDI and air temperature verifies the hypothesis that conditions of higher surface moisture (the TVDI value tends toward 0) are locally associated with lower values of air temperature, while the conditions of lower surface moisture (the TVDI value tends toward 1) are associated with higher values of air temperature (**Figure 20**). **Figure 20** shows that the locations at which in situ observations were made are predominantly wet surfaces (TVDI < 0.50). That did not permit the assessment of the relationship between the TVDI and in situ observations of air temperature and relative humidity in drier conditions.

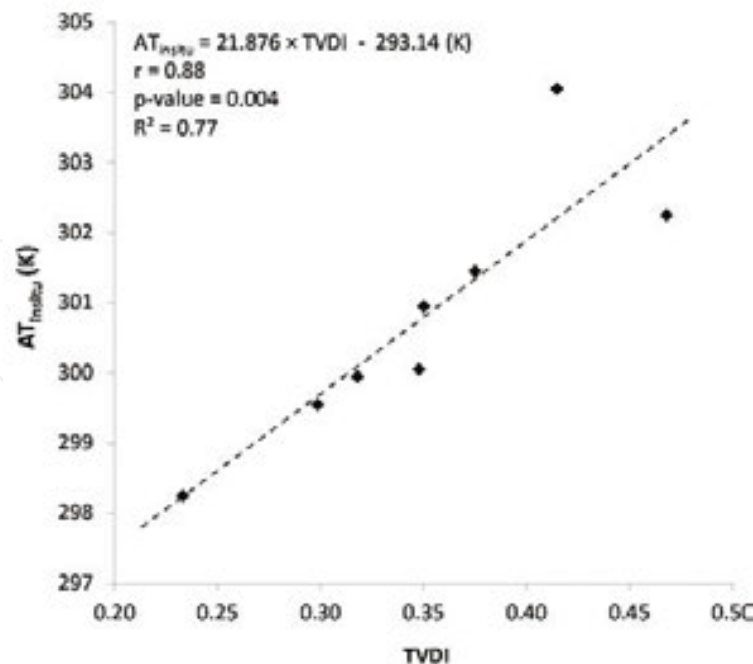


Figure 20. Correlation between the temperature/vegetation dryness index (TVDI) derived from airborne imagery and in situ observations of air temperature (AT).

4. Discussion

4.1. Vegetation index and percent vegetation cover

The NDVI estimated using airborne multispectral imaging ($NDVI_{\text{airborne}}$) is an important indicator of the spatial heterogeneity of agricultural surfaces and their intra-plot variability. It allows the easy distinguishing of different states of agricultural lands like full vegetation cover, partial vegetation cover, and bare soil. NDVI values which are associated with these thematic classes were, respectively, estimated at 0.58 (SD = 0.087), 0.37 (SD = 0.172), and 0.10 (SD = 0.071) for vegetable crops on organic soil. These values are close to those observed in different studies using in situ observations if we consider the bias of 0.118 between $NDVI_{\text{airborne}}$ and $NDVI_{\text{in situ}}$. For example, Van De Griend and Owe [92] report a value of 0.157 for the NDVI of bare soil (sandy loam). Considering all potential sources of error mentioned above and the uncertainty of NDVI values reported by different studies [106], the uncertainty of ± 0.045 of $NDVI_{\text{airborne}}$ is satisfactory. Nagol [106] reports NDVI uncertainty values varying between ± 0.023 and ± 0.085 according to different types of vegetation and weather conditions. Compared to NDVI, PVC refers more to a vegetation cover rate and a quantity of biomass. Full cover vegetation has a maximum PVC value and an absence of vegetation have a zero value. Thus, PVC allows a better characterization of the amount of vegetation, from bare soil to full vegetation cover. This characterization would allow a better assessment of phenological stages.

4.2. Airborne infrared thermography, surface temperature of agricultural lands and crop management

The estimation of ST using airborne infrared thermography (ST_{airborne}) allowed the characterization of the intra-plot variability of agricultural lands over the study area. This variability is mainly associated with a variation in the percent vegetation cover, the type of vegetation, surface moisture conditions, and different types of soil. ST_{airborne} thus helps to reveal the changing microclimate conditions across crop fields. It is a useful variable for the modeling and estimation of MCIs at local scales. And it offers a high potential for crop management given its ability to detect problematic areas in the field. The ST_{airborne} was estimated with an uncertainty of ± 0.73 K and a bias of 1.42 K with respect to in situ observations. The uncertainty of ST_{airborne} is greater than the sensitivity of the infrared thermography camera (± 0.007 K), but its estimated bias is lower than the accuracy of the camera (2.00 K). The uncertainty of ST_{airborne} is due to the measurement accuracy of the camera, the uncertainty of the surface emissivity estimated by using in-situ observations and airborne multispectral imagery, the uncertainty of the atmospheric correction, and the uncertainties of the orthorectification and image mosaicking. The uncertainty of ST_{airborne} is relatively good considering all these sources of uncertainties. Some conditions and components of the method helped to achieve this good result in the present study: (1) the clear sky during the acquisition of the airborne images, (2) the low altitude used for this acquisition which resulted in a low optical thickness, and (3) the mapping of surface emissivity which helped to reduce the influence of the main source of uncertainty in the estimation of the ST_{airborne} . The estimation of ST_{airborne} in clear sky conditions with a relatively low uncertainty, aligns with the observations of Moran et al. [107] who report

that in these conditions where visibility is high and water vapor content is low, the atmospheric correction of thermal images is not necessary because the absorption by atmospheric particles is balanced by the thermal emission of these components. The uncertainty and the bias of the ST_{airborne} is close to those of the ST estimated using other airborne sensors [108–110] or earth observation satellites [108, 111–116]. Considering the high intra-plot variability of ST, even if on full cover vegetation surfaces, the uncertainty of ST_{airborne} is satisfactory to characterize the microclimate conditions of agricultural lands. Using airborne infrared thermography is a promising approach to characterizing agricultural surfaces and a promising diagnostic and decision-making tool for crop management. This allows the characterization of growing conditions along with the occurrence and behavior of diseases and pests through the estimation of several other MCIs like surface humidity and near surface air temperature.

4.3. The TVDI indicator of surface moisture

The trapezoidal space ST/NDVI and the TVDI estimated using airborne multispectral imaging and infrared thermography allowed a good characterization of the spatial variability of surface moisture and its temporal variability induced by successive acquisition flight lines. The variation of humidity conditions over the study area, from the wet limit to the dry one, is thus both time and space dependent. This study shows that the ST/NDVI space and the limit lines defining the TVDI could be established on an intra-seasonal and inter-seasonal basis to assess surface moisture and could take into account not only prevailing moisture conditions at the time of image acquisition but also taking into account the dynamics of these conditions throughout the season and between seasons. The concept of sub-cloud points of wet and dry limits of the ST/NDVI space and their clear identification were used to improve the estimation of those limit lines and to assess their uncertainty. The use of sub-cloud points reduces the subjectivity of the estimation of the limit lines by calculating their uncertainty. Wang et al. [63] report about this subjectivity and the imprecision that it generates in the estimation of the TVDI. The concept of the sub-cloud points of the limit lines allows the assessment of this imprecision and allows this to be taken into account when estimating the uncertainty of the TVDI. The TVDI was estimated over the study area with a low uncertainty. The analysis of the components of this uncertainty showed that it is strongly related to the NDVI and the temperature of the dry limit. The uncertainty of the TVDI increases with the NDVI, and it decreases with the temperature of the dry limit. Each of these two variables allows a full expression of the minimum and maximum uncertainty of the TVDI for a given percent vegetation cover. These results confirm those of Li et al. [21] who also report that the uncertainty of the TVDI increases with the NDVI and the approximation of the isolines. The TVDI showed that the intra-plot variability of surface moisture may be quite high on vegetable crop surfaces. Of two neighboring fields, the spatial extent of one can be mainly characterized by surface moisture conditions close to those of the wet limit while that of the other one can be mainly characterized by surface moisture conditions close to those of the dry limit. This reflects the high spatial variability of the agro-meteorological conditions that could influence the abundance of crop diseases and pests in the fields.

4.4. Added value of the integration of optical and microwave data for the characterization of microclimatic conditions and crop identification

The integration of microwave remote sensing data (passive or active) with optical (multispectral) and thermal data offers several advantages both for the characterization of microclimatic conditions and for the characterization of land use and land cover (LULC). This integration makes it possible to characterize both the microclimatic conditions of the surface (surface temperature and moisture) and the air near the surface (near surface air temperature) by using optical and thermal remote sensing data and the microclimatic conditions of the soil layers near the surface (soil temperature and moisture) by using microwave remote sensing data.

Soil temperature and soil moisture are two important agro-meteorological variables. The first has an influence on both the development of crops and several pests and pathogenic microorganisms in the soil. The second is more directly related to the water content of the soil, and thus to the amount of water available for the development and growth of crops. But in the conditions of the presence of vegetation and cloud cover, it is more difficult to estimate these two variables using optical and thermal remote sensing data. Indeed, in the presence of vegetation, surface temperature and moisture estimated by optical and thermal data are more related to the canopy or to a mixed surface composed of canopy and fraction of bare soil, while microwave remote sensing data offer a better potential for estimating soil temperature and soil humidity even in the presence of vegetation (low vegetation percent cover) and clouds [117–120]. For example, Manns et al. [118] used data from the airborne sensor Passive Active L-band System (PALS) to estimate soil moisture in agricultural and forest areas. However, some disadvantages are associated with the use of microwave remote sensing for estimating soil temperature or soil moisture depends on the type of system used. The major one is the low spatial resolution of passive microwave sensors [117, 119]. The use of radar sensors (active microwave) has the advantage of a better spatial resolution compared to passive microwave sensors. However, the estimation of soil moisture using radar images is more difficult because these data are more sensitive to the surface roughness and to the structure of the canopy [117].

Different crop varieties may have different canopy structures (size and geometry of the canopy, canopy density, leaf orientation, row direction) at certain phenological stages [121]. As the radar remote sensing data are highly sensitive to this structural variation [117], their integration with optical data acquired at specific periods of the season optimizes the accuracy of the algorithms used to perform classification of crops [121].

4.5. About the use of airborne-based technologies versus spaceborne-based technologies

Airborne data offer many advantages for the characterization of microclimatic conditions, identification of different crop varieties, and monitoring of crop condition and phenology. One of the most important advantages is the flexibility of the choice of spatial resolution, spectral resolution, and temporal resolution at which the images will be acquired.

Compared to satellite images for which the spatial, temporal, and spectral resolutions are already set, those of airborne images can be defined according to the needs and constraints of the user. For example, very high spatial resolution images can be acquired at particular periods

of the season and at specific times of the day to meet precise needs in agriculture. However, the spatial, temporal, and spectral resolutions of satellite images would not allow to do so.

The growing interest in the use of drones for remote sensing applications and their rapid development open the way for a greater access to airborne imagery with reducing acquisition costs (aircraft rent and pilot fees, flight authorization, etc.), increasing autonomy (the purchase of a drone and the expertise to operate it are more accessible compared to an aircraft), and reducing constraints related to airborne mission (minimum permitted flight height, the spatial resolution increases with the decrease of the flight height).

5. Conclusion

Infrared thermography and airborne multispectral imaging were used in this study to estimate surface microclimate indicators (SMIs) at local scale and to assess their uncertainties. Normalized difference vegetation index (NDVI), percent vegetation cover (PVC), surface temperature (ST) and the temperature/vegetation dryness index (TVDI) were used to characterize local and intra-plot variability of the amount of vegetation, the surface temperature, and surface moisture. The ST estimated by airborne infrared thermography offers a high potential for the management of vegetable crops, as it allows the detection and investigation of problematic zones in the fields. The spatial variability of surface temperature has been associated with several growth factors and management practices of agricultural lands such as soil type (mineral soil, black earth, loam), drainage and soil quality, soil moisture, crop varieties and their growth stage, and stress (water and nutrient deficit, abiotic damage). This thermal variability is the result of several agro-meteorological phenomena that govern crop yields, as well as the occurrence and behavior of crop pests and diseases. The TVDI demonstrated that intra-plot variability of surface moisture may be quite high on crop surfaces. This reflects the high variability of microclimate conditions that can affect diseases and pests that are present on these surfaces. The main limitation of the applications of SMIs derived from airborne remote sensing is the cost of images acquisition and processing. Planning airborne missions and using unmanned aerial vehicles (UAV) via a shared service that includes different stakeholders working in the same territory (agricultural producers, agroenvironmental consulting clubs, phytosanitary warning networks, etc.) would be able to meet the specific needs of crop management and integrated pest management (spatial and temporal resolution, periods and critical management areas), while significantly reducing the costs associated with the use of such data. Moreover, the rapid development of technologies related to Earth observation satellites and sensors has led to better spatial and temporal resolutions. The growing availability of Earth observation images due to a greater number of satellites in orbit, the advent of satellite constellations, and various integrated Earth observation programs will allow for greater frequency of image acquisition over vast territories and at finer scales. This will help reduce data gaps and enable better monitoring of microclimate and agrometeorological conditions at local scales.

Acknowledgements

This work is a part of the thesis study of the first author. It was carried out with the financial support of the Natural Sciences and Engineering Research Council of Canada (NSERC) and the Compagnie de Recherche Phytodata Inc., PRISME Consortium, Sherrington, Québec, Canada through the Industrial Postgraduate Scholarships (IPS) program. Thanks to Stéphanie Bourgon, Jocelyn Bluteau, Gilles Lavoie, Richard Picard, Guido Castellanos, Bakary Koné, and Aliou Diouf, all from Université Laval, for their help in acquisition and processing of GPS data, measurement of in situ meteorological and spectroradiometric data, and planning and acquisition of airborne remote sensing images. We also thank the staff of the PRISME Consortium, especially Luc Brodeur, Gerardo Gollo Gill, Caesar Chlela, Abdenour Boukhalfa, Mohammed Boudache, and Franck Bosquain who facilitated our research residency within their organization and supported our collection of data in the field.

Author details

Serge Olivier Kotchi^{1,2,3*}, Nathalie Barrette^{2,4}, Alain A. Viau^{2,3}, Jae-Dong Jang⁵, Valéry Gond⁶ and Mir Abolfazl Mostafavi^{2,3}

*Address all correspondence to: serge-olivier.kotchi@phac-aspc.gc.ca

1 National Microbiology Laboratory (NML), Public Health Agency of Canada (PHAC), Saint-Hyacinthe, Quebec, Canada

2 Faculty of Forestry, Geography and Geomatics, Laval University, Quebec City, Quebec, Canada

3 Center for Research in Geomatics (CRG), Laval University, Quebec City, Quebec, Canada

4 Hydro-Quebec Institute in Environment, Development and Society (EDS Institute), Laval University, Quebec City, Quebec, Canada

5 National Meteorological Satellite Center (NMSC), Korean Meteorological Administration (KMA), Jincheon, South Korea

6 French Agricultural Research Centre for International Development (CIRAD), Montpellier, France

References

- [1] Carisse O, Tremblay D-M, McDonald MR, Brodeur L, McRoberts N. Management of botrytis leaf blight of onion: the Québec experience of 20 years of continual improvement. *Plant Disease*. 2011;95(5):504–14.
- [2] Dalla Marta A, Magarey RD, Orlandini S. Modelling leaf wetness duration and downy mildew simulation on grapevine in Italy. *Agricultural and Forest Meteorology*. 2005;132(1–2):84–95.
- [3] Gordon TR, Koike ST. Management of Fusarium wilt of lettuce. *Crop Protection*. 2015;73:45–9.
- [4] Park Y-L, Krell RK, Carroll M. Theory, technology, and practice of site-specific insect pest management. *Journal of Asia-Pacific Entomology*. 2007;10(2):89–101.
- [5] Whitfield GH, Carruthers RI, Haynes DL. Phenology and control of the onion maggot (Diptera: Anthomyiidae) in Michigan onion production. *Agriculture, Ecosystems & Environment*. 1985;12(3):189–200.
- [6] Wu BM, Subbarao KV, van Bruggen AHC. Analyses of the relationships between lettuce downy mildew and weather variables using geographic information system techniques. *Plant Disease*. 2005;89(1):90–6.
- [7] Hoogenboom G. Contribution of agrometeorology to the simulation of crop production and its applications. *Agricultural and Forest Meteorology*. 2000;103(1–2):137–57.
- [8] Delamater PL, Messina JP, Qi J, Cochrane MA. A hybrid visual estimation method for the collection of ground truth fractional coverage data in a humid tropical environment. *International Journal of Applied Earth Observation and Geoinformation*. 2012;18:504–14.
- [9] Ju C, Cai T, Yang X. Topography-based modeling to estimate percent vegetation cover in semi-arid Mu Us sandy land, China. *Computers and Electronics in Agriculture*. 2008;64(2):133–9.
- [10] Sentelhas PC, Dalla Marta A, Orlandini S, Santos EA, Gillespie TJ, Gleason ML. Suitability of relative humidity as an estimator of leaf wetness duration. *Agricultural and Forest Meteorology*. 2008;148(3):392–400.
- [11] Dalezios NR, Loukas A, Bampzelis D. The role of agrometeorological and agrohydrological indices in the phenology of wheat in central Greece. *Physics and Chemistry of the Earth, Parts A/B/C*. 2002;27(23–24):1019–23.
- [12] Pou A, Diago MP, Medrano H, Baluja J, Tardaguila J. Validation of thermal indices for water status identification in grapevine. *Agricultural Water Management*. 2014;134:60–72.

- [13] Sentelhas PC, Gillespie TJ, Santos EA. Evaluation of FAO Penman–Monteith and alternative methods for estimating reference evapotranspiration with missing data in Southern Ontario, Canada. *Agricultural Water Management*. 2010;97(5):635–44.
- [14] Erdem Y, Arin L, Erdem T, Polat S, Deveci M, Okursoy H, et al. Crop water stress index for assessing irrigation scheduling of drip irrigated broccoli (*Brassica oleracea* L. var. *italica*). *Agricultural Water Management*. 2010;98(1):148–56.
- [15] Gontia NK, Tiwari KN. Development of crop water stress index of wheat crop for scheduling irrigation using infrared thermometry. *Agricultural Water Management*. 2008;95(10):1144–52.
- [16] Du L, Tian Q, Yu T, Meng Q, Jancso T, Udvardy P, et al. A comprehensive drought monitoring method integrating MODIS and TRMM data. *International Journal of Applied Earth Observation and Geoinformation*. 2013;23:245–53.
- [17] Kuśmierk-Tomaszewska R, Żarski J, Dudek S. Meteorological automated weather station data application for plant water requirements estimation. *Computers and Electronics in Agriculture*. 2012;88:44–51.
- [18] Benali A, Carvalho AC, Nunes JP, Carvalhais N, Santos A. Estimating air surface temperature in Portugal using MODIS LST data. *Remote Sensing of Environment*. 2012;124:108–21.
- [19] Chen T, Niu RQ, Wang Y, Zhang LP, Du B. Percentage of vegetation cover change monitoring in Wuhan region based on remote sensing. *Procedia Environmental Sciences*. 2011;10, Part B:1466–72.
- [20] Deng C, Wu C. Estimating very high resolution urban surface temperature using a spectral unmixing and thermal mixing approach. *International Journal of Applied Earth Observation and Geoinformation*. 2013;23:155–64.
- [21] Li Z, Wang Y, Zhou Q, Wu J, Peng J, Chang H. Spatiotemporal variability of land surface moisture based on vegetation and temperature characteristics in Northern Shaanxi Loess Plateau, China. *Journal of Arid Environments*. 2008;72(6):974–85.
- [22] Mondal P, Jain M, DeFries RS, Galford GL, Small C. Sensitivity of crop cover to climate variability: Insights from two Indian agro-ecoregions. *Journal of Environmental Management*. 2015;148:21–30.
- [23] Orlandini S, Massetti L, Marta AD. An agrometeorological approach for the simulation of *Plasmopara viticola*. *Computers and Electronics in Agriculture*. 2008;64(2):149–61.
- [24] Zhang F, Zhang L-W, Shi J-J, Huang J-F. Soil moisture monitoring based on land surface temperature-vegetation index space derived from MODIS data. *Pedosphere*. 2014;24(4):450–60.

- [25] Abraha MG, Savage MJ. Comparison of estimates of daily solar radiation from air temperature range for application in crop simulations. *Agricultural and Forest Meteorology*. 2008;148(3):401–16.
- [26] Ehret DL, Hill BD, Helmer T, Edwards DR. Neural network modeling of greenhouse tomato yield, growth and water use from automated crop monitoring data. *Computers and Electronics in Agriculture*. 2011;79(1):82–9.
- [27] Garcia y Garcia A, Guerra LC, Hoogenboom G. Impact of generated solar radiation on simulated crop growth and yield. *Ecological Modelling*. 2008;210(3):312–26.
- [28] Kross A, McNairn H, Lapen D, Sunohara M, Champagne C. Assessment of RapidEye vegetation indices for estimation of leaf area index and biomass in corn and soybean crops. *International Journal of Applied Earth Observation and Geoinformation*. 2015;34:235–48.
- [29] Cicogna A, Dietrich S, Gani M, Giovanardi R, Sandra M. Use of meteorological radar to estimate leaf wetness as data input for application of territorial epidemiological model (downy mildew – *Plasmopara viticola*). *Physics and Chemistry of the Earth, Parts A/B/C*. 2005;30(1–3):201–7.
- [30] Moonen AC, Ercoli L, Mariotti M, Masoni A. Climate change in Italy indicated by agrometeorological indices over 122 years. *Agricultural and Forest Meteorology*. 2002;111(1):13–27.
- [31] Paterson RRM, Sariah M, Lima N. How will climate change affect oil palm fungal diseases? *Crop Protection*. 2013;46:113–20.
- [32] Marques da Silva JR, Damásio CV, Sousa AMO, Bugalho L, Pessanha L, Quaresma P. Agriculture pest and disease risk maps considering MSG satellite data and land surface temperature. *International Journal of Applied Earth Observation and Geoinformation*. 2015;38:40–50.
- [33] Vancutsem C, Ceccato P, Dinku T, Connor SJ. Evaluation of MODIS land surface temperature data to estimate air temperature in different ecosystems over Africa. *Remote Sensing of Environment*. 2010;114(2):449–65.
- [34] Rahimzadeh-Bajgiran P, Omasa K, Shimizu Y. Comparative evaluation of the vegetation dryness index (VDI), the temperature vegetation dryness index (TVDI) and the improved TVDI (iTVDI) for water stress detection in semi-arid regions of Iran. *ISPRS Journal of Photogrammetry and Remote Sensing*. 2012;68:1–12.
- [35] de Wit AJW, Boogaard HL, van Diepen CA. Using NOAA-AVHRR estimates of land surface temperature for regional agrometeorological modelling. *International Journal of Applied Earth Observation and Geoinformation*. 2004;5(3):187–204.
- [36] Seiler RA, Kogan F, Wei G, Vinocur M. Seasonal and interannual responses of the vegetation and production of crops in Cordoba–Argentina assessed by AVHRR derived vegetation indices. *Advances in Space Research*. 2007;39(1):88–94.

- [37] Corbari C, Bissolati M, Mancini M. Multi-scales and multi-satellites estimates of evapotranspiration with a residual energy balance model in the Muzza agricultural district in Northern Italy. *Journal of Hydrology*. 2015;524:243–54.
- [38] Wu W, Liu H-B, Hoogenboom G, White JW. Evaluating the accuracy of VEMAP daily weather data for application in crop simulations on a regional scale. *European Journal of Agronomy*. 2010;32(3):187–94.
- [39] Doraiswamy PC, Pasteris PA, Jones KC, Motha RP, Nejedlik P. Techniques for methods of collection, database management and distribution of agrometeorological data. *Agricultural and Forest Meteorology*. 2000;103(1–2):83–97.
- [40] Laurence H, Fabry F, Dutilleul P, Bourgeois G, Zawadzki I. Estimation of the spatial pattern of surface relative humidity using ground based radar measurements and its application to disease risk assessment. *Agricultural and Forest Meteorology*. 2002;111(3):223–31.
- [41] Sentelhas PC, Gillespie TJ, Gleason ML, Monteiro JEBM, Pezzopane JRM, Pedro Jr MJ. Evaluation of a Penman–Monteith approach to provide “reference” and crop canopy leaf wetness duration estimates. *Agricultural and Forest Meteorology*. 2006;141(2–4): 105–17.
- [42] Gonzalez-Dugo V, Zarco-Tejada PJ, Fereres E. Applicability and limitations of using the crop water stress index as an indicator of water deficits in citrus orchards. *Agricultural and Forest Meteorology*. 2014;198–199:94–104.
- [43] Cruz-Blanco M, Lorite IJ, Santos C. An innovative remote sensing based reference evapotranspiration method to support irrigation water management under semi-arid conditions. *Agricultural Water Management*. 2014;131:135–45.
- [44] De Pauw E, Göbel W, Adam H. Agrometeorological aspects of agriculture and forestry in the arid zones. *Agricultural and Forest Meteorology*. 2000;103(1–2):43–58.
- [45] He Y. The effect of precipitation on vegetation cover over three landscape units in a protected semi-arid grassland: Temporal dynamics and suitable climatic index. *Journal of Arid Environments*. 2014;109:74–82.
- [46] Jin H, Eklundh L. A physically based vegetation index for improved monitoring of plant phenology. *Remote Sensing of Environment*. 2014;152:512–25.
- [47] Eckert S, Engesser M. Assessing vegetation cover and biomass in restored erosion areas in Iceland using SPOT satellite data. *Applied Geography*. 2013;40:179–90.
- [48] Nagler PL, Glenn EP, Huete AR. Assessment of spectral vegetation indices for riparian vegetation in the Colorado River delta, Mexico. *Journal of Arid Environments*. 2001;49(1):91–110.

- [49] Du Q, Chang N-B, Yang C, Srilakshmi KR. Combination of multispectral remote sensing, variable rate technology and environmental modeling for citrus pest management. *Journal of Environmental Management*. 2008;86(1):14–26.
- [50] Duchemin B, Hadria R, Erraki S, Boulet G, Maisongrande P, Chehbouni A, et al. Monitoring wheat phenology and irrigation in Central Morocco: On the use of relationships between evapotranspiration, crops coefficients, leaf area index and remotely-sensed vegetation indices. *Agricultural Water Management*. 2006;79(1):1–27.
- [51] Liu J, Pattey E, Jégo G. Assessment of vegetation indices for regional crop green LAI estimation from Landsat images over multiple growing seasons. *Remote Sensing of Environment*. 2012;123:347–58.
- [52] Pan Z, Huang J, Zhou Q, Wang L, Cheng Y, Zhang H, et al. Mapping crop phenology using NDVI time-series derived from HJ-1 A/B data. *International Journal of Applied Earth Observation and Geoinformation*. 2015;34:188–97.
- [53] Dong J, Xiao X, Wagle P, Zhang G, Zhou Y, Jin C, et al. Comparison of four EVI-based models for estimating gross primary production of maize and soybean croplands and tallgrass prairie under severe drought. *Remote Sensing of Environment*. 2015;162:154–68.
- [54] Er-Raki S, Rodriguez JC, Garatuza-Payan J, Watts CJ, Chehbouni A. Determination of crop evapotranspiration of table grapes in a semi-arid region of Northwest Mexico using multi-spectral vegetation index. *Agricultural Water Management*. 2013;122:12–9.
- [55] Bolton DK, Friedl MA. Forecasting crop yield using remotely sensed vegetation indices and crop phenology metrics. *Agricultural and Forest Meteorology*. 2013;173:74–84.
- [56] Holzman ME, Rivas R, Piccolo MC. Estimating soil moisture and the relationship with crop yield using surface temperature and vegetation index. *International Journal of Applied Earth Observation and Geoinformation*. 2014;28:181–92.
- [57] Wang Y, Zia S, Owusu-Adu S, Gerhards R, Müller J. Early detection of fungal diseases in winter wheat by multi-optical sensors. *APCBEE Procedia*. 2014;8:199–203.
- [58] Romano G, Zia S, Spreer W, Sanchez C, Cairns J, Araus JL, et al. Use of thermography for high throughput phenotyping of tropical maize adaptation in water stress. *Computers and Electronics in Agriculture*. 2011;79(1):67–74.
- [59] Ghosh A, Joshi PK. Hyperspectral imagery for disaggregation of land surface temperature with selected regression algorithms over different land use land cover scenes. *ISPRS Journal of Photogrammetry and Remote Sensing*. 2014;96:76–93.
- [60] Wu P, Shen H, Zhang L, Göttsche F-M. Integrated fusion of multi-scale polar-orbiting and geostationary satellite observations for the mapping of high spatial and temporal resolution land surface temperature. *Remote Sensing of Environment*. 2015;156:169–81.

- [61] Sruthi S, Aslam MAM. Agricultural drought analysis using the NDVI and land surface temperature data; a case study of Raichur District. *Aquatic Procedia*. 2015;4:1258–64.
- [62] Garcia M, Fernández N, Villagarcía L, Domingo F, Puigdefábregas J, Sandholt I. Accuracy of the temperature–vegetation dryness index using MODIS under water-limited vs. energy-limited evapotranspiration conditions. *Remote Sensing of Environment*. 2014;149:100–17.
- [63] Wang H, Li X, Long H, Xu X, Bao Y. Monitoring the effects of land use and cover type changes on soil moisture using remote-sensing data: A case study in China's Yongding River basin. *Catena*. 2010;82(3):135–45.
- [64] Chen C-F, Son N-T, Chang L-Y, Chen C-C. Monitoring of soil moisture variability in relation to rice cropping systems in the Vietnamese Mekong Delta using MODIS data. *Applied Geography*. 2011;31(2):463–75.
- [65] Schwarz N, Lautenbach S, Seppelt R. Exploring indicators for quantifying surface urban heat islands of European cities with MODIS land surface temperatures. *Remote Sensing of Environment*. 2011;115(12):3175–86.
- [66] Pan Y, Li L, Zhang J, Liang S, Zhu X, Sulla-Menashe D. Winter wheat area estimation from MODIS-EVI time series data using the Crop Proportion Phenology Index. *Remote Sensing of Environment*. 2012;119:232–42.
- [67] Crowder DW, Harwood JD. Promoting biological control in a rapidly changing world. *Biological Control*. 2014;75:1–7.
- [68] Qin Z, Zhang M. Detection of rice sheath blight for in-season disease management using multispectral remote sensing. *International Journal of Applied Earth Observation and Geoinformation*. 2005;7(2):115–28.
- [69] Tripathy AK, Adinarayana J, Vijayalakshmi K, Merchant SN, Desai UB, Ninomiya S, et al. Knowledge discovery and leaf spot dynamics of groundnut crop through wireless sensor network and data mining techniques. *Computers and Electronics in Agriculture*. 2014;107:104–14.
- [70] Matese A, Crisci A, Di Gennaro SF, Primicerio J, Tomasi D, Marcuzzo P, et al. Spatial variability of meteorological conditions at different scales in viticulture. *Agricultural and Forest Meteorology*. 2014;189–190:159–67.
- [71] Wood GA, Taylor JC, Godwin RJ. Calibration methodology for mapping within-field crop variability using remote sensing. *Biosystems Engineering*. 2003;84(4):409–23.
- [72] Lamb DW, Brown RB. PA--precision agriculture: Remote-sensing and mapping of weeds in crops. *Journal of Agricultural Engineering Research*. 2001;78(2):117–25.
- [73] Akasheh OZ, Neale CMU, Jayanthi H. Detailed mapping of riparian vegetation in the middle Rio Grande River using high resolution multi-spectral airborne remote sensing. *Journal of Arid Environments*. 2008;72(9):1734–44.

- [74] Zhang H, Lan Y, Suh CPC, Westbrook J, Clint Hoffmann W, Yang C, et al. Fusion of remotely sensed data from airborne and ground-based sensors to enhance detection of cotton plants. *Computers and Electronics in Agriculture*. 2013;93:55–9.
- [75] Agam N, Cohen Y, Berni JAJ, Alchanatis V, Kool D, Dag A, et al. An insight to the performance of crop water stress index for olive trees. *Agricultural Water Management*. 2013;118:79–86.
- [76] Ramos JG, Cratchley CR, Kay JA, Casterad MA, Martínez-Cob A, Domínguez R. Evaluation of satellite evapotranspiration estimates using ground-meteorological data available for the Flumen District into the Ebro Valley of N.E. Spain. *Agricultural Water Management*. 2009;96(4):638–52.
- [77] Government of Canada. Canadian Digital Elevation Data (CDED). In: Natural Resources Canada, Earth Sciences Sector, Centre for Topographic Information, editors. Sherbrooke, Quebec, Canada: Centre for Topographic Information; 2000.
- [78] Gitin AV. Radiometry of optical systems with quasi-homogeneous sources: A linear systems approach. *Optik – International Journal for Light and Electron Optics*. 2011;122(19):1713–8.
- [79] Pasher J, King DJ. Multivariate forest structure modelling and mapping using high resolution airborne imagery and topographic information. *Remote Sensing of Environment*. 2010;114(8):1718–32.
- [80] Doutre C, Nasiopoulos P, editors. Fast vignetting correction and color matching for panoramic image stitching. 16th IEEE International Conference on Image Processing (ICIP); November 7–10, 2009; Cairo, Egypt.
- [81] Hasler D, Süsstrunk S. Mapping colour in image stitching applications. *Journal of Visual Communication and Image Representation*. 2004;15(1):65–90.
- [82] Smith GM, Milton EJ. The use of the empirical line method to calibrate remotely sensed data to reflectance. *International Journal of Remote Sensing*. 1999;20:2653–62.
- [83] Moran MS, Bryant R, Thome K, Ni W, Nouvellon Y, Gonzalez-Dugo MP, et al. A refined empirical line approach for reflectance factor retrieval from Landsat-5 TM and Landsat-7 ETM+. *Remote Sensing of Environment*. 2001;78(1–2):71–82.
- [84] Xu JF, Huang JF. Refined empirical line method to calibrate IKONOS imagery. *Journal of Zhejiang University – Science A*. 2006;7(4):641–6.
- [85] Matlock TS, Hargus WA, Larson CW. Thermographic Characterization and Comparison of 200 W and 600 W Hall Thrusters. Ft. Belvoir: Defense Technical Information Center; 2007; Available from: <http://handle.dtic.mil/100.2/ADA471080>.
- [86] Holst GC. *Common Sense Approach to Thermal Imaging*. Winter Park, FL, Bellingham, WA: JCD Pub.; co-published by SPIE Optical Engineering Press; 2000. xiii, 377 pp.

- [87] Jensen JR. *Introductory Digital Image Processing: A Remote Sensing Perspective*. 3rd ed. Upper Saddle River, NJ: Prentice Hall; 2005. xv, 526 pp.
- [88] Sun J, Yang J, Zhang C, Yun W, Qu J. Automatic remotely sensed image classification in a grid environment based on the maximum likelihood method. *Mathematical and Computer Modelling*. 2013;58(3–4):573–81.
- [89] Smits PC, Dellepiane SG, Schowengerdt RA. Quality assessment of image classification algorithms for land-cover mapping: A review and a proposal for a cost-based approach. *International Journal of Remote Sensing*. 1999;20(8):1461–86.
- [90] Skirvin SM, Kepner WG, Marsh SE, Drake SE, Maingi JK, Edmonds CM, et al. Assessing the accuracy of satellite-derived land-cover classification using historical aerial photography, digital orthophoto quadrangles, and airborne video data. In: Lunetta R, Lyon JG, editors. *Remote Sensing and GIS Accuracy Assessment*. Boca Raton, FL: CRC Press; 2004. p. 115–31.
- [91] Rouse JW, Haas RH, Schell JA, Deering DW, Harlan JC. Monitoring the vernal advancements and retrogradation (greenwave effect) of nature vegetation. Texas A&M Univ.; Remote Sensing Center.; College Station, TX, United States: National Aeronautics and Space Administration (NASA), 1974 Contract No.: NAS5–21857.
- [92] Van De Griend AA, Owe M. On the relationship between thermal emissivity and the normalized difference vegetation index for natural surfaces. *International Journal of Remote Sensing*. 1993;14(6):1119–31.
- [93] Dalezios NR, Loukas A, Bampzelis D. Assessment of NDVI and agrometeorological indices for major crops in central Greece. *Physics and Chemistry of the Earth, Parts A/B/C*. 2002;27(23–24):1025–9.
- [94] Carlson TN, Ripley DA. On the relation between NDVI, fractional vegetation cover, and leaf area index. *Remote Sensing of Environment*. 1997;62(3):241–52.
- [95] ISO. *Uncertainty of measurement – Part 3: Guide to the expression of uncertainty in measurement (GUM:1995)*. Geneva, Switzerland: International Organization for Standardization (ISO), ISO/IEC Guide 98–3:2008, 2008.
- [96] Bonn F, Rochon G. *Précis de télédétection. Volume 1, Principes et méthodes*. Sainte-Foy: Presses de l'Université du Québec; 1992.
- [97] Bonn F, Escadafal R. *La télédétection appliquée aux sols*. In: Presses de l'université du Québec, editor. *Précis de télédétection, Volume 2, applications thématiques*. Sainte-Foy/Montréal: Bonn, F.; 1996. p. 633 pages.
- [98] Sobrino JA, Raissouni N. Toward remote sensing methods for land cover dynamic monitoring: Application to Morocco. *International Journal of Remote Sensing*. 2000;21(2):353–66.

- [99] Minkina W, Dudzik S. *Infrared Thermography: Errors and Uncertainties*. Chippenham, Wiltshire, Great Britain: John Wiley & Sons; 2009. Available from: <http://onlinelibrary.wiley.com/book/10.1002/9780470682234>.
- [100] Hamrelius T. Accurate Temperature-Measurement in Thermography – an Overview of Relevant Features, Parameters and Definitions. *Proceedings of the Society of Photo-Optical Instrumentation Engineers (SPIE)*. 1991;1467:448-57.
- [101] Sandholt I, Rasmussen K, Andersen J. A simple interpretation of the surface temperature/vegetation index space for assessment of surface moisture status. *Remote Sensing of Environment*. 2002;79(2-3):213-24.
- [102] Gao Z, Gao W, Chang N-B. Integrating temperature vegetation dryness index (TVDI) and regional water stress index (RWSI) for drought assessment with the aid of LANDSAT TM/ETM+ images. *International Journal of Applied Earth Observation and Geoinformation*. 2011;13(3):495-503.
- [103] Liu Z, Shi X, Warner E, Ge Y, Yu D, Ni S, et al. Relationship between oriental migratory locust plague and soil moisture extracted from MODIS data. *International Journal of Applied Earth Observation and Geoinformation*. 2008;10(1):84-91.
- [104] Naira C, Robert L, Ramata M, Marouane T. Surface soil moisture status over the Mackenzie River Basin using a temperature/vegetation index. *Geoscience and Remote Sensing Symposium, 2007 IGARSS 2007 IEEE International* [Internet]. 2007, pp. 1846-8 pp. Available from: <http://ieeexplore.ieee.org/stamp/stamp.jsp?tp=&arnumber=4423182&isnumber=4422708>.
- [105] Xin J, Tian G, Liu Q, Chen L. Combining vegetation index and remotely sensed temperature for estimation of soil moisture in China. *International Journal of Remote Sensing*. 2006;27:2071-5.
- [106] Nagol JR. Quantification of error in AVHRR NDVI data [thesis]. College Park, Maryland: University of Maryland; 2011.
- [107] Moran MS, Inoue Y, Barnes EM. Opportunities and limitations for image-based remote sensing in precision crop management. *Remote Sensing of Environment*. 1997;61(3):319-46.
- [108] Coll C, Caselles V, Rubio E, Sospedra F, Valor E. Temperature and emissivity separation from calibrated data of the digital airborne imaging spectrometer. *Remote Sensing of Environment*. 2001;76(2):250-9.
- [109] Rahkonen J, Jokela H. Infrared radiometry for measuring plant leaf temperature during thermal weed control treatment. *Biosystems Engineering*. 2003;86(3):257-66.
- [110] Wanjura DF, Upchurch DR. Infrared thermometer calibration and viewing method effects on canopy temperature-measurement. *Agricultural and Forest Meteorology*. 1991;55(3-4):309-21.

- [111] Kerr YH, Lagouarde JP, Imbernon J. Accurate land surface-temperature retrieval from AVHRR data with use of an improved split window algorithm. *Remote Sensing of Environment*. 1992;41(2-3):197–209.
- [112] Li ZL, Tang BH, Wu H, Ren HZ, Yan GJ, Wan ZM, et al. Satellite-derived land surface temperature: Current status and perspectives. *Remote Sensing of Environment*. 2013;131:14–37.
- [113] Mallick J, Singh CK, Shashtri S, Rahman A, Mukherjee S. Land surface emissivity retrieval based on moisture index from LANDSAT TM satellite data over heterogeneous surfaces of Delhi city. *International Journal of Applied Earth Observation and Geoinformation*. 2012;19:348–58.
- [114] Niclòs R, Galve JM, Valiente JA, Estrela MJ, Coll C. Accuracy assessment of land surface temperature retrievals from MSG2-SEVIRI data. *Remote Sensing of Environment*. 2011;115(8):2126–40.
- [115] Norman JM, Divakarla M, Goel NS. Algorithms for extracting information from remote thermal-IR observations of the earth's surface. *Remote Sensing of Environment*. 1995;51(1):157–68.
- [116] Srivastava PK, Majumdar TJ, Bhattacharya AK. Surface temperature estimation in Singhbhum Shear Zone of India using Landsat-7 ETM+ thermal infrared data. *Advances in Space Research*. 2009;43(10):1563–74.
- [117] Lee WS, Alchanatis V, Yang C, Hirafuji M, Moshou D, Li C. Sensing technologies for precision specialty crop production. *Computers and Electronics in Agriculture*. 2010;74(1):2–33.
- [118] Manns HR, Berg AA, Colliander A. Soil organic carbon as a factor in passive microwave retrievals of soil water content over agricultural croplands. *Journal of Hydrology*. 2015;528:643–51.
- [119] Merlin O, Chehbouni A, Kerr YH, Goodrich DC. A downscaling method for distributing surface soil moisture within a microwave pixel: Application to the Monsoon '90 data. *Remote Sensing of Environment*. 2006;101(3):379–89.
- [120] Moran MS, Vidal A, Troufleau D, Qi J, Clarke TR, Pinter Jr PJ, et al. Combining multifrequency microwave and optical data for crop management. *Remote Sensing of Environment*. 1997;61(1):96–109.
- [121] McNairn H, Champagne C, Shang J, Holmstrom D, Reichert G. Integration of optical and synthetic aperture radar (SAR) imagery for delivering operational annual crop inventories. *ISPRS Journal of Photogrammetry and Remote Sensing*. 2009;64(5):434–49.

